Electromagnetic separators (3)

Ulli Köster

Institut Laue-Langevin
Grenoble, France

Addendum: atomic spectroscopy of astatine

Author	Year	Method	IP (eV)
Finkelnburg *et al.*[10]	1950	Extrapolation	9.5(2)
Varshni *et al.*[11]	1953	Extrapolation	10.4
Finkelnburg *et al.*[12]	1955	Extrapolation	9.2(4)
Kiser *et al.*[13]	1960	Extrapolation	9.5
Mitin *et al.*[14]	2006	HF	9.24
Chang *et al.*[15]	2010	MCDF, up-shift	9.35(1)

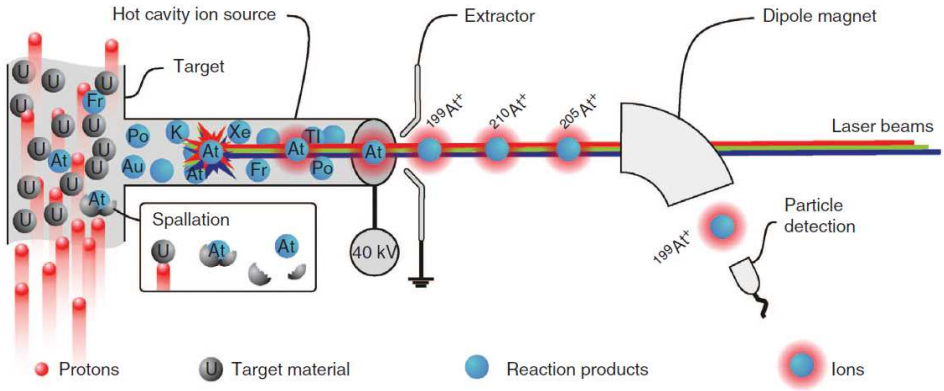

S. Rothe et al., Nature Comm. 4 (2013) 1835.

Addendum: atomic spectroscopy of astatine

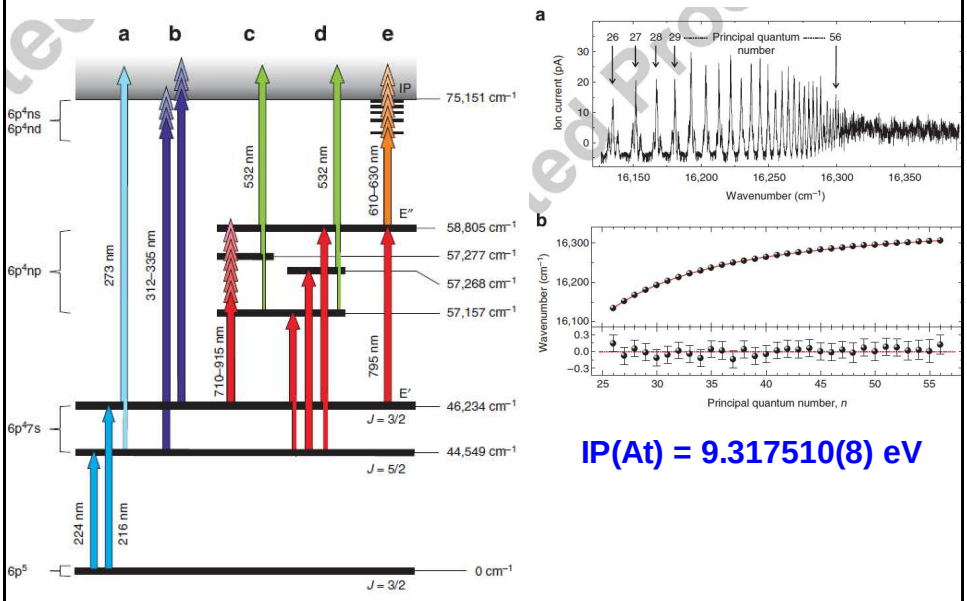

IP(At) = 9.317510(8) eV

S. Rothe et al., Nature Comm. 4 (2013) 1835.

Outline

1. Definitions and history
2. Basics of ion **optics and dispersive elements**
3. Static fields
   a) deflection spectrometer
   b) retardation spectrometer
4. Dynamic fields/separation
   a) Time-of-Flight spectrometer
   b) Radiofrequency spectrometer
   c) Traps
5. Technical realization (ion sources, etc.)
6. **"Real examples" for nuclear physics applications**
   a) ISOL
   b) Recoil separators
   c) Fragment separators
   d) Spectrometer

Types of commercial mass spectrometers

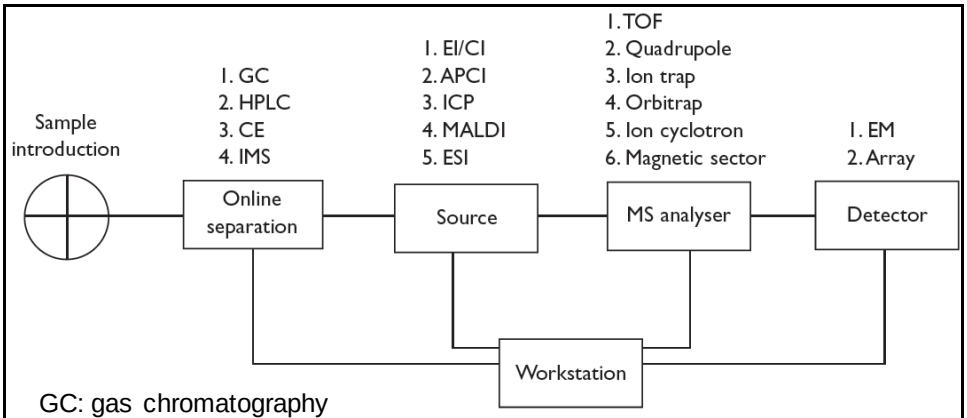

GC: gas chromatography
HPLC: high pressure liquid chromatography
CE: capillary electrophoresis
IMS: ion mobility spectroscopy
EI/CI: electron impact/chemical ionization
APCI: atmospheric pressure chem. ioniz.
ICP: inductively coupled plasma
MALDI: matrix assisted laser desorption/ioniz.
ESI: electrospray ionization

S. Naylor and P.T. Babcock, Drug Discovery World (Fall 2010) 73.

Inductively Coupled Plasma-MS

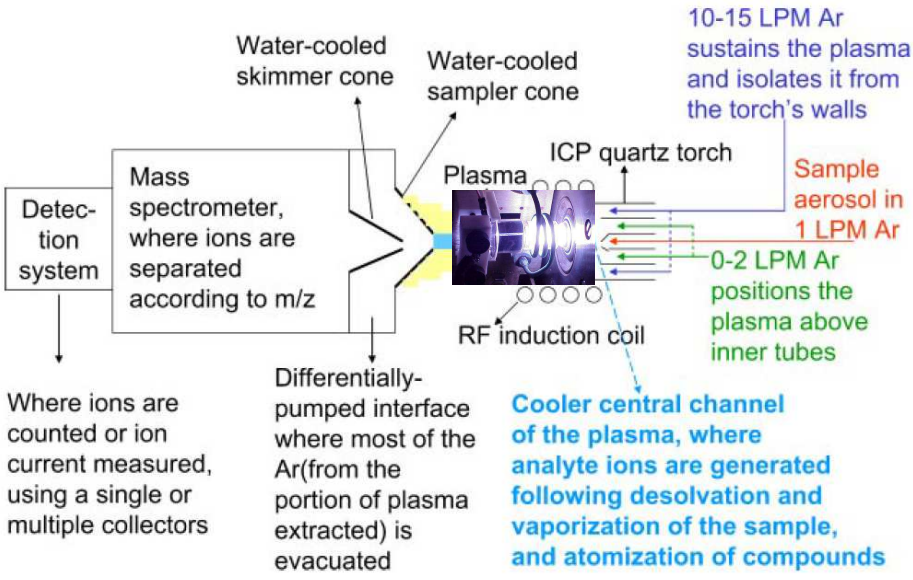

D. Beauchemin, Mass Spectrom. Rev. 29 (2010) 560.

TOF-SIMS
time-of-flight secondary ion mass spectrometer

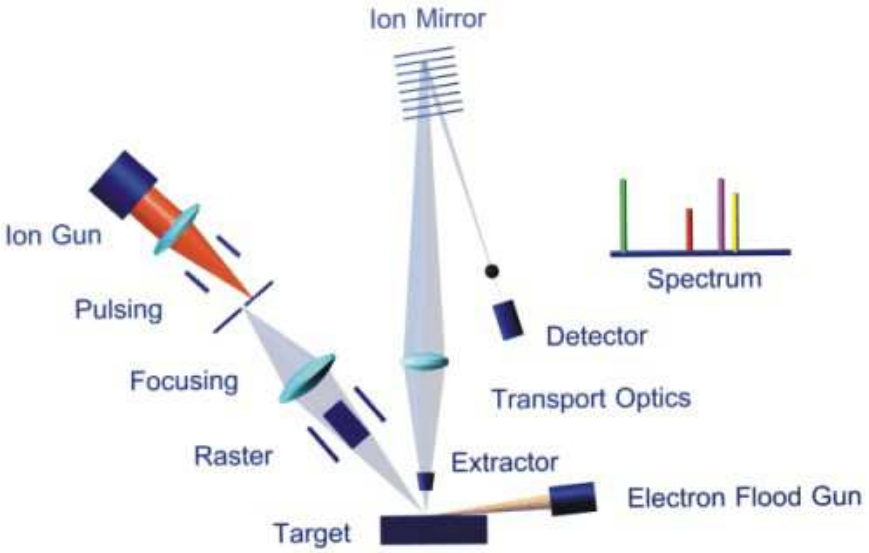

MALDI-TOF
matrix assisted laser desorption/ionization TOF

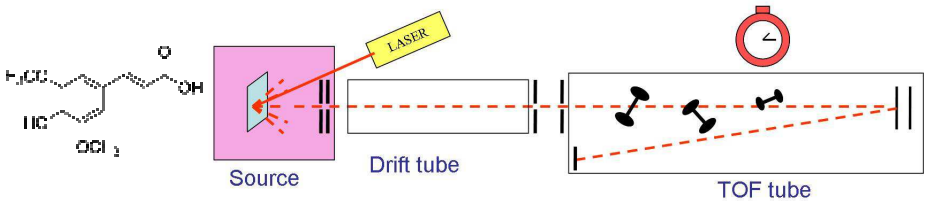

Matrix:
- low vapor pressure for operation at low pressure
- polar groups for use in aqueous solutions
- strong absorption in UV or IR for efficient evaporation by laser
- low molecular weight for easy evaporation
- acidic: provides easily protons for ionization of analyte

Mass selectivity of radio-frequency quadrupoles

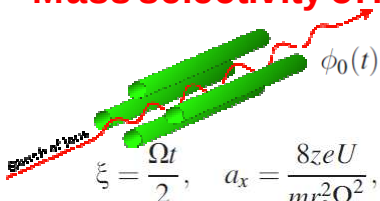

$$\phi_0(t) = U - V_{RF}\cos\Omega t$$

$$\xi = \frac{\Omega t}{2}, \quad a_x = \frac{8zeU}{mr_0^2\Omega^2}, \quad q_x = \frac{4zeV_{RF}}{mr_0^2\Omega^2}$$

$$\frac{d^2x}{d\xi^2} + (a_x - 2q_x\cos 2\xi)x = 0$$

Mathieu equation

$$a_y = -a_x, \quad q_y = -q_x$$

$m_1 < m_2 < m_3$

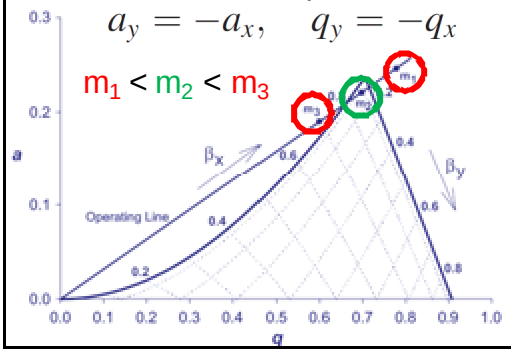

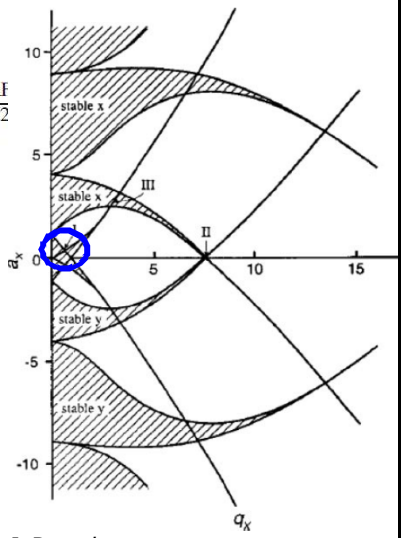

D.J. Douglas, Mass Spectrom. Rev. 28 (2009) 937.

Orbitrap

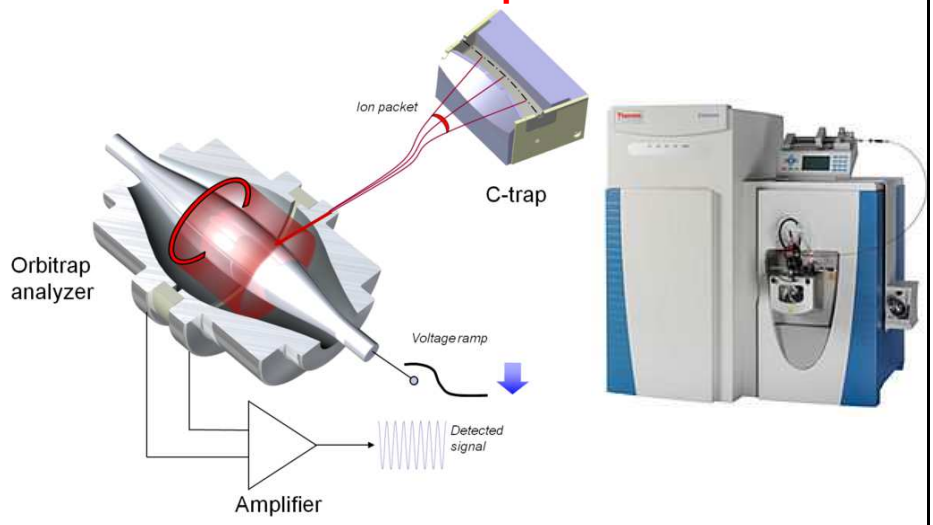

- coaxial spindle-like electrodes form dynamic trapping field
- image current from ions > Fourier transformation > frequency > mass

A. Makarov, Anal. Chem. 72 (2000) 1156.

Ultrahigh-mass mass spectrometry

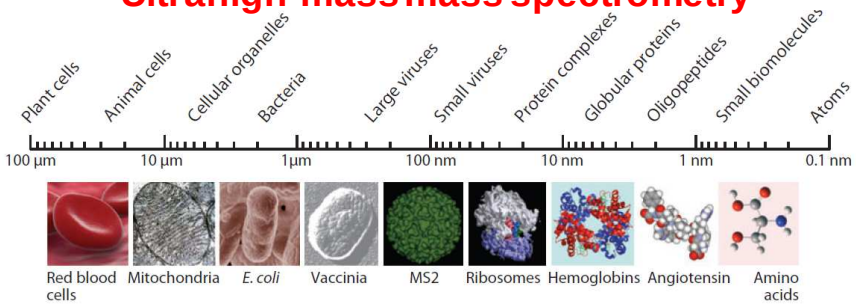

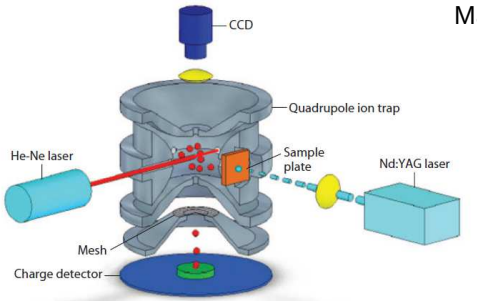

Mass distribution of human erythrocytes

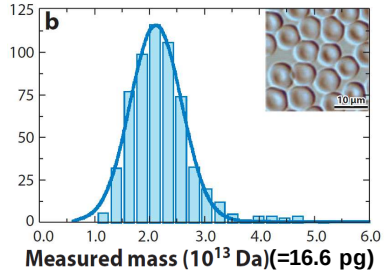

H.-C. Chang, Annu. Rev. Anal. Chem. 2 (2009) 169.

Forensic applications

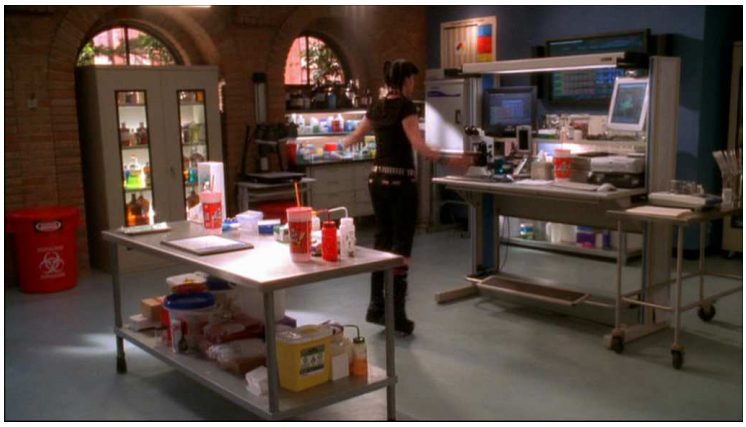

- trace detection of drugs, poisons, explosives, etc.
- composition analysis of paint, tissue, etc.
- pesticide control
- measurement of isotopic composition
- etc.

Doping control

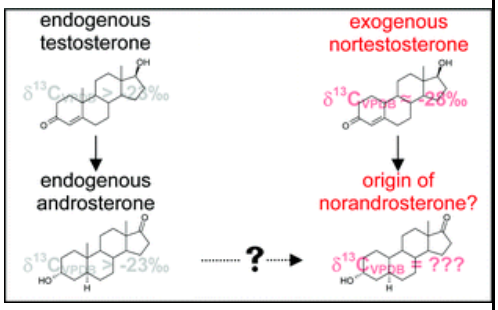

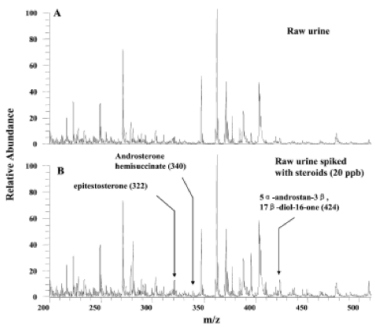

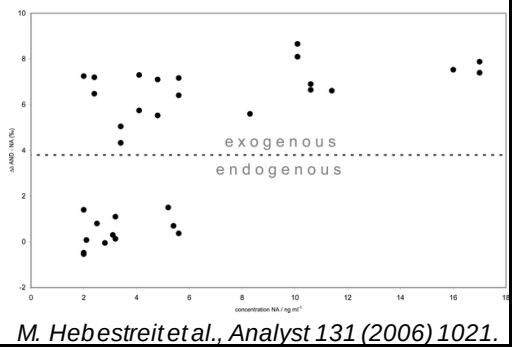

M. Hebestreit et al., Analyst 131 (2006) 1021.

Radiocarbon dating

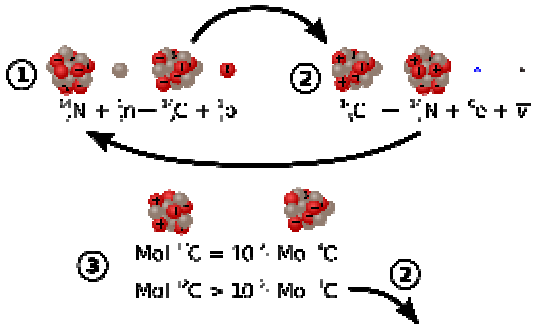

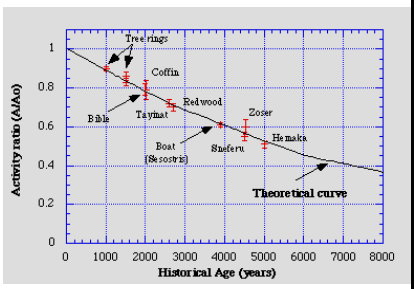

- Cosmic radiation > spallation neutrons > $^{14}N(n,p)^{14}C$ reactions
- Living organisms: equilibrium with atmospheric $^{14}C/^{12}C$ ratio
- After death: $^{14}C/^{12}C$ decreases due to ^{14}C decay ($T_{1/2}$=5370 y)

Problem: measure $^{14}C^{+}$ at ppt level without interference from
$^{14}N^{+}$, $^{12}CH_2^{+}$, $^{13}CH^{+}$, $^{28}Si^{++}$, $^{12}C^{16}O^{++}$, $^{42}Ca^{+++}$, $^{56}Fe^{++++}$,…

Multistep-Separation in Accelerator Mass Spectrometry

1. Negative ion formation — $^{14}N^{-}$ anions do not exist
2. Acceleration and stripping — breakup of molecules
3. Z-selective ion detector — $\frac{dE}{dx} \sim \frac{Z^2}{E}$

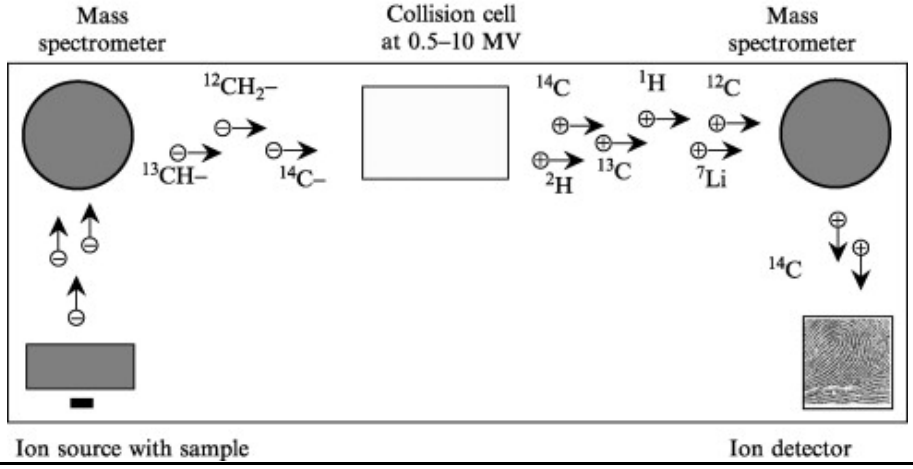

Age calibration

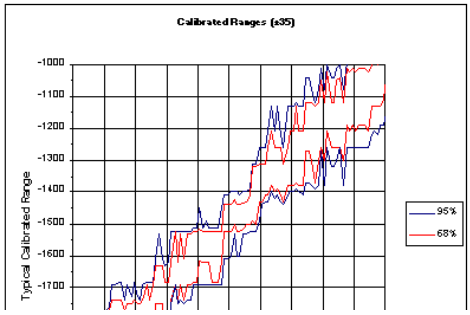

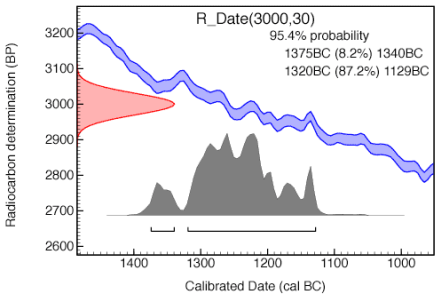

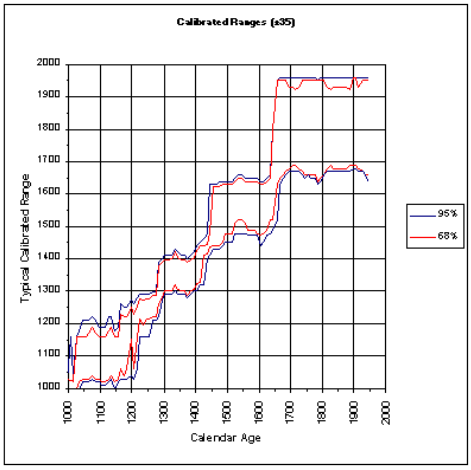

The shroud of Turin AD 1260-1390

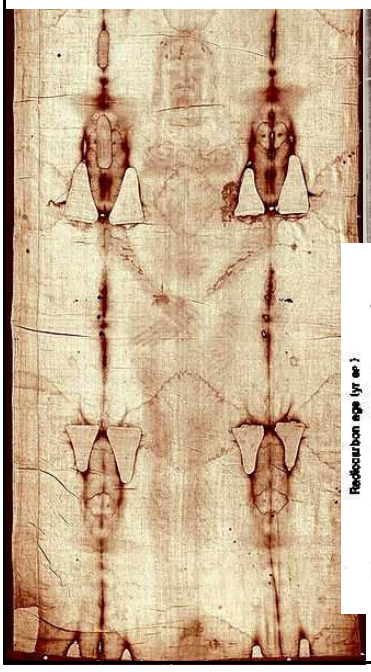

AMS measurements at Arizona, Oxford and Zurich.

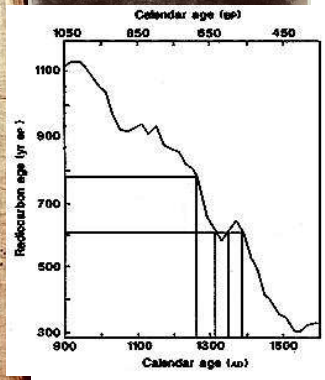

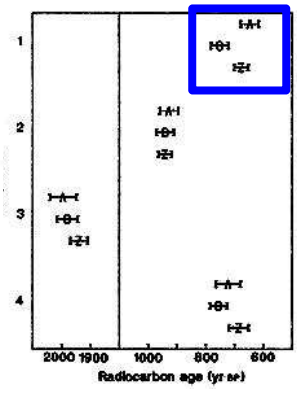

P.E. Damon et al., Nature 337 (1989) 611.

Aerosol composition in Swiss alpine valleys

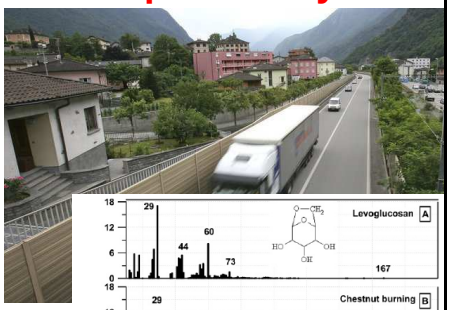

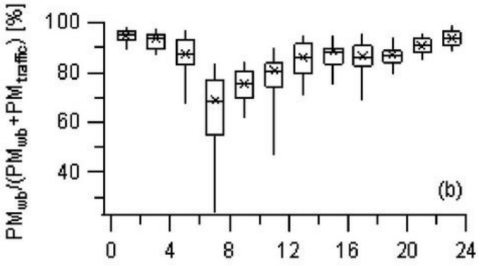

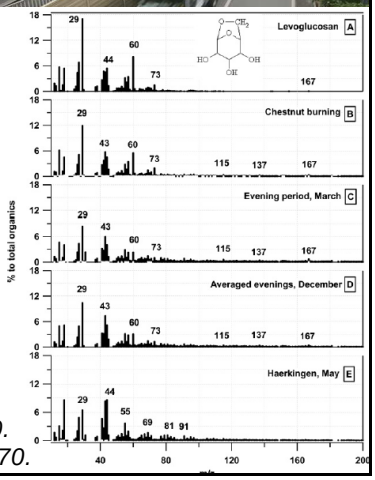

S. Szidat et al., Geophys. Res. Lett. 34 (2007) L05820.
M.R. Alfarra et al., Environ. Sci. Technol. 41 (2007) 5770.

Asian haze: biomass burning contributes !

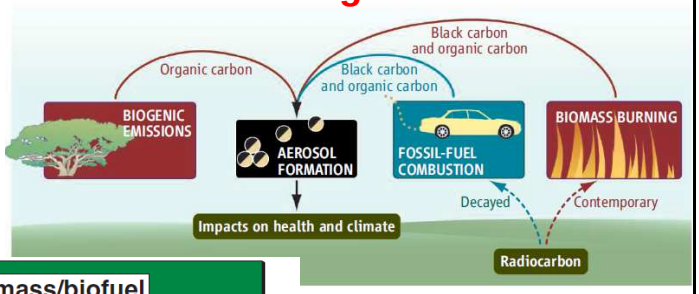

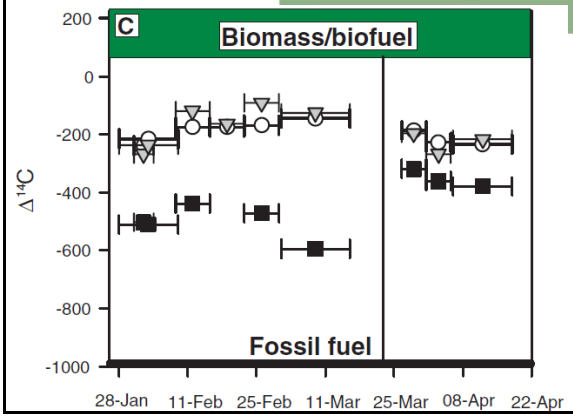

S. Szidat, Science 323 (2009) 470.
Ö. Gustafsson et al., Science 323 (2009) 495.

6 MV tandem: the "working horse" for AMS

ETH Zürich, Laboratory for Ion Beam Physics

0.6 MV TANDY: the "working pony" for AMS

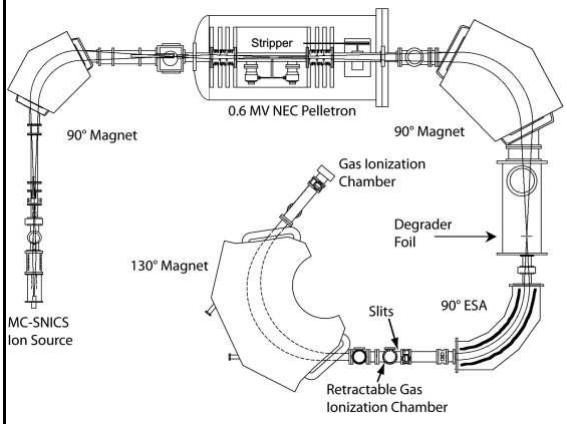

Routine measurements of: ^{10}Be, ^{41}Ca, ^{129}I, ^{236}U, Pu, etc.
longer-lived than ^{14}C: geology, cosmochronology,…

ETH Zürich, Laboratory for Ion Beam Physics

MICADAS (Mini-radioCArbon-DAting-System): 0.2 MV AMS

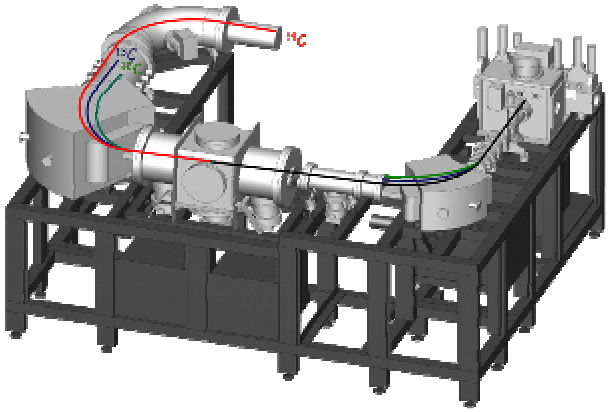

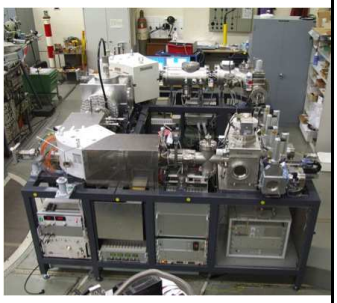

2.3 x 3 m^2 "tabletop"

Routine measurements of: ^{14}C

ETH Zürich, Laboratory for Ion Beam Physics

MUCADAS (MICRO-radioCArbon-DAting-System): 45 kV AMS

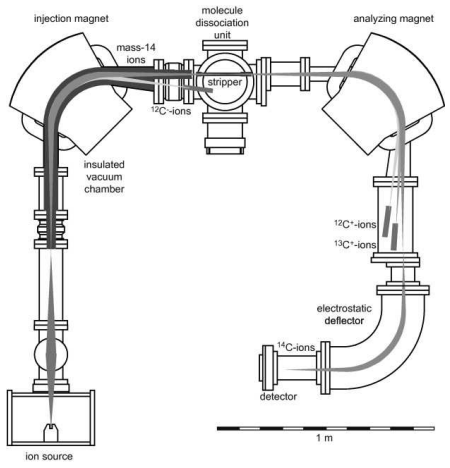

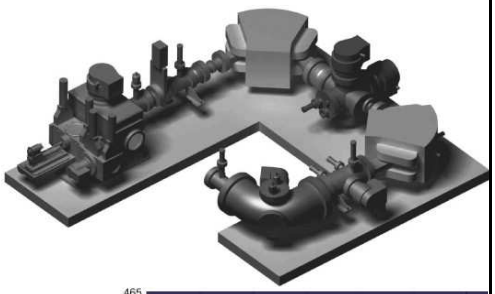

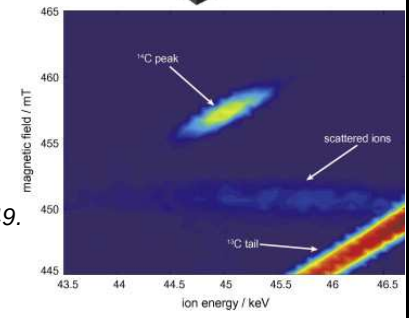

H.A. Synal et al., Nucl. Instr. Meth. B294 (2013) 349.

ETH Zürich, Laboratory for Ion Beam Physics

Retardation spectrometer

- electrostatic energy measurement
- charged particles move against electrostatic potential; transmission measured as function of repulsive potential
- analyzes only the energy component perpendicular to the analyzer
- total energy measurement requires perfectly parallel beam

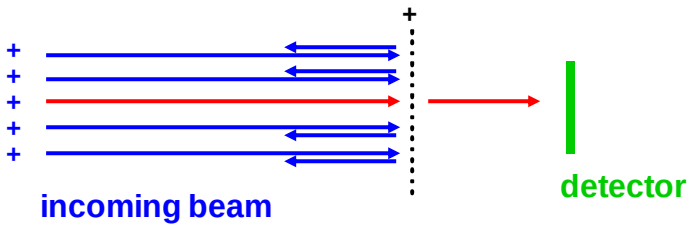

Examples of MAC-E retardation spectrometer

1. WITCH at ISOLDE: weak interaction studies via recoil detection after EC/β^+ decay
2. ASPECT at ILL: precision spectroscopy of angular correlation between neutron spin and decay protons
3. KATRIN in Karlsruhe: precision measurement of beta endpoint in tritium decay for neutrino mass determination

ß-decay and neutrino mass

model independent neutrino mass from ß-decay kinematics

$$\frac{d\Gamma_i}{dE} = C\,p\,(E+m_e)\,(E_0-E)\,\sqrt{(E_0-E)^2-m_i^2}\,F(E)\,\theta(E_0-E-m_i)$$

$$C = G_F^2\frac{m_e^5}{2\pi^3}\cos^2\theta_C\,|M|^2$$

experimental observable is m_ν^2

E_0 = 18.6 keV
$T_{1/2}$ = 12.3 y

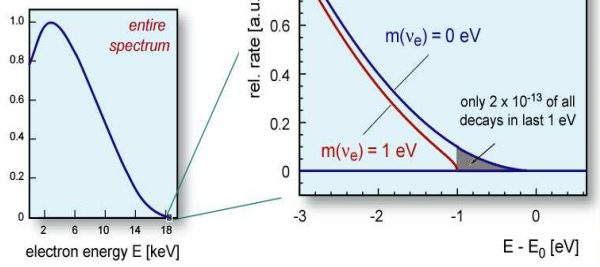

ß-source requirements:

- high ß-decay rate (short $t_{1/2}$)
- low ß-endpoint energy E_0
- superallowed ß-transition
- few inelastic scatters of ß's

ß-detection requirements:

- high resolution ($\Delta E <$ few eV)
- large solid angle ($\Delta\Omega \sim 2\pi$)
- low background

Electrostatic filter with Magnetic Adiabatic Collimation

MAC-E-Technique

adiabatic guiding of ß-particles along the magnetic field lines

inhomogen. B-Feld: stray field of 2 super-conducting magnets

B_{max} = 3 - 6 T

B_{min} < 1 mT

very large solid angle !

$\Delta\Omega \sim 2\pi$

$\vec{F} = (\vec{\mu}\cdot\vec{\nabla})\,\vec{B} + q\,\vec{E}$

$\mu = E_\perp / B = \text{const}$

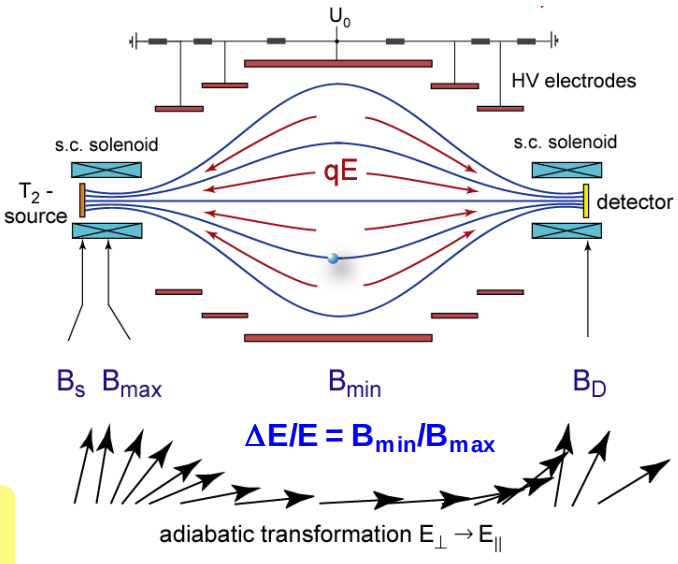

A. Picard et al., Nucl. Instr. Meth. B63 (1992) 345.

KATRIN experiment

Karlsruhe **Tri**tium **N**eutrino Experiment

at Forschungszentrum Karlsruhe

unique facility for closed T_2 cycle: Tritium Laboratory Karlsruhe

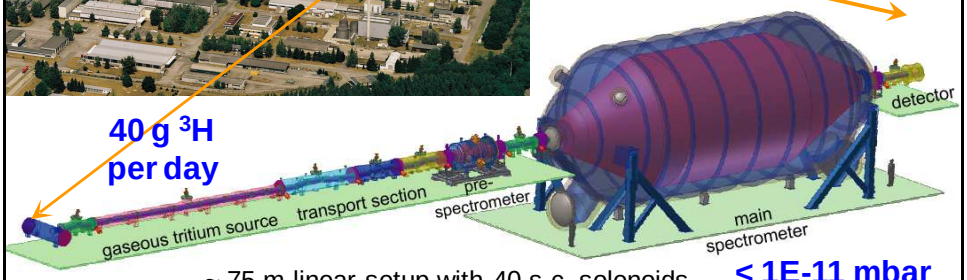

~ 75 m linear setup with 40 s.c. solenoids

< 1E-11 mbar
< 1E-20 mbar ³H

main spectrometer – design

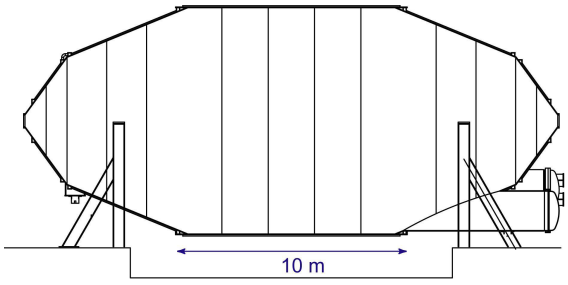

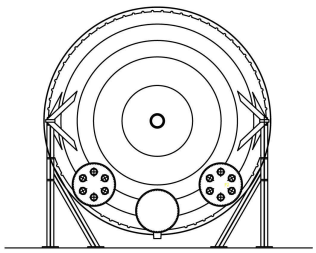

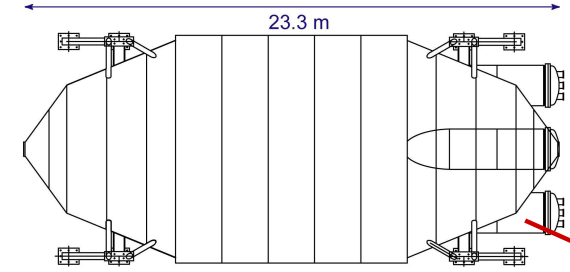

design parameters:

volume:	1258 m^3
surface:	605 m^2
thickness:	32 mm
material	1.4429
weight:	192 t

pumping port for getters


UNITED KINGDOM
IRELAND
Belfast
Dublin
Irish Sea
Isle of Man (U.K.)
Leeds
Manchester
Liverpool
Birmingham
Cardiff
London
Celtic Sea
Guernsey (U.K.)
Jersey (U.K.)
Bay of Biscay
FRANCE
Paris
Nantes
Loire
Brussels
Lille
BEL.
Bonn
GERMANY
Frankfurt am Main
Luxembourg
LUX.
Strasbourg
Stuttgart
Munich
Essen
Cologne
Leipzig
Hamburg
Bremen
Berlin
Amsterdam
NETH.
Rotterdam
Rhine
Elbe
Oder
Poznań
Warsaw
POLAND
Łódź
Wrocław
Vistula
Gdańsk
Bornholm
Copenhagen
Malmö
DENMARK
Sea
Kaliningrad
RUSSIA
Vilnius
LITHUANIA
Minsk
Mahilyow
BELARUS
Hrodna
Brest
Homyel'
Kiev
Rivne
Dnieper
UKRAINE
L'viv
Kraków
Prague
CZECH REPUBLIC
Brno
SLOVAKIA
Bratislava
Vienna
AUSTRIA
LIECH.
Zürich
Bern
SWITZ.
Vaduz
Geneva
Budapest
HUNGARY
Cluj-Napoca
Chernivtsi
Mykolayiv
Chişinău
Iaşi
MOLDOVA
ROMANIA
Bucharest
Constanta
Black Sea
Varna
Danube
Ljubljana
SLOVENIA
Zagreb
Milan
Venice
Turin
Lyon
MASSIF CENTRAL
Bordeaux
Belgrade
BOSNIA AND HERZEGOVINA
CROATIA
Sarajevo
Serbia
BULGARIA
Sofia
Skopje
Istanbul
Bursa
Izmir
TURKEY
Aegean Sea
Thessaloniki
Tirana
ALB.
Podgorica
Montenegro
Adriatic Sea
Ligurian Sea
Florence
Genoa
SAN MARINO
MONACO
Marseille
Toulouse
Andorra la Vella
ANDORRA
PYRENEES
Bilbao
Porto
PORTUGAL
Zaragoza
Madrid
Barcelona
Corsica
ITALY
Rome
VATICAN CITY
Naples
Tyrrhenian Sea
Ionian Sea
GREECE
Athens
Crete
Rhodes
Lisbon
Tagus
SPAIN
Valencia
Balearic Sea
Sardinia
BALEARIC ISLANDS
Cagliari
Palermo
Sicily
Sevilla
Gibraltar (U.K.)
Málaga
Strait of Gibraltar
Ceuta (SPAIN)
Alborán Sea
Mediterranean Sea
Algiers
Melilla (SPAIN)
Oran
Tunis
TUNISIA
Valletta
MALTA
Rabat
Casablanca
MOROCCO
ALGERIA
Scale 1: 19,500,000
Lambert Conformal Conic Projection, standard parallels 40°N and 56°N
0 300 Kilometers
0 20 300 Miles

Identification ≠ Separation

- **Identification:**
  The beam composition is determined but not changed.
  e.g. time-of-flight measurement, ΔE measurement,...

- **Separation:**
  Beam contaminations are removed.
  e.g. mass separation, chemical separation,...

- **Unique isotope selection** requires the combination of **at least two** different identification/separation methods.

- A **higher-fold** combination gives improved suppression factors.

Prism

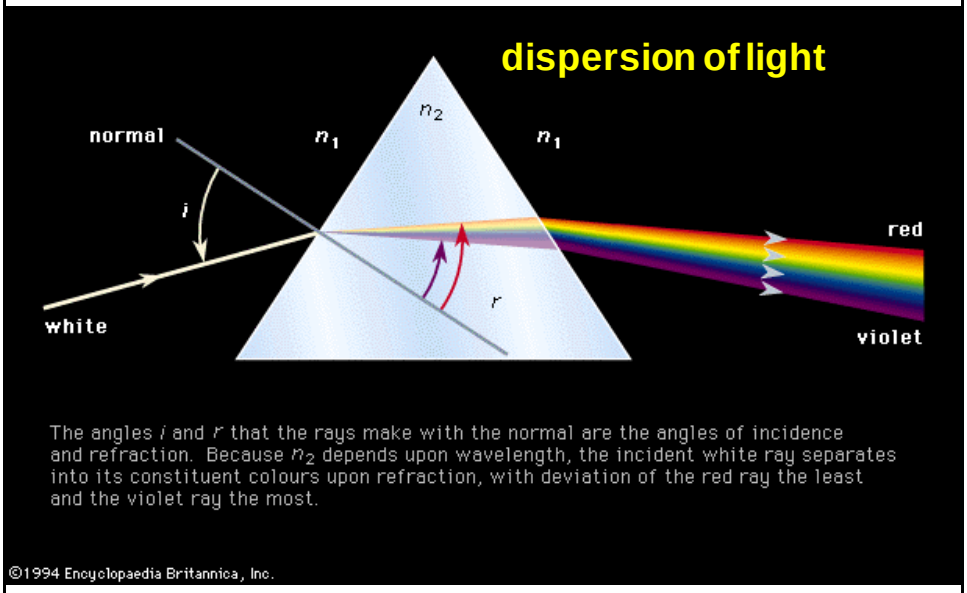

Dispersive ion optical elements

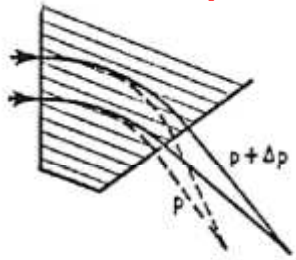

FIG. 5.15 A system with momentum dependent deflection of the central ray, showing lateral displacement due to momentum spread.

- magnets are momentum dispersive
- electrostatic deflectors are energy dispersive
- Wien filters are velocity dispersive

Focusing by tilted entrance/exit of magnetic field

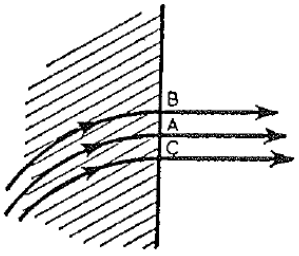

FIG. 5.3 Particles leaving a magnetic field normal to the edge.

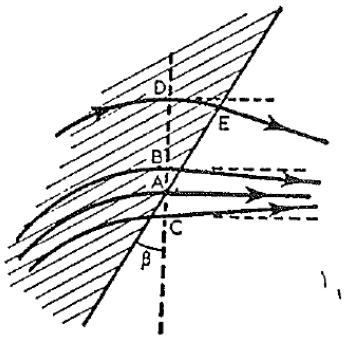

FIG. 5.4 Particles leaving a magnetic field at an angle to the edge. Dotted lines are for normal exit (cf. Fig. 5.3).

horizontal focusing effect

Focusing by tilted entrance/exit of magnetic field

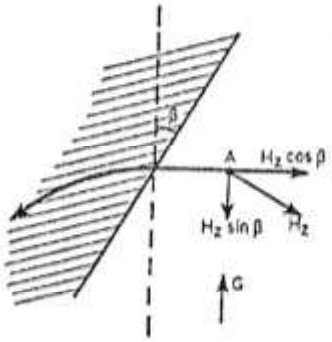

FIG. 5.5 Plan view of a positively charged particle entering a magnetic field directed into the paper. The trajectory makes an angle β with the normal. For view in the direction of arrow G see Fig. 5.6.

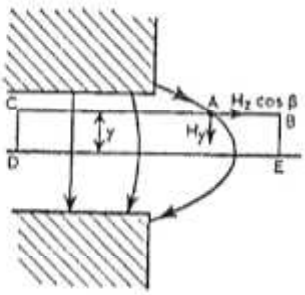

FIG. 5.6 View of Fig. 5.5 in the direction of arrow G. DE is the median plane on which $H_z = 0$.

vertical defocusing effect

Quadrupoles

Electrostatic:

$V = U\,(x^2 - y^2)/a^2$

$\mathcal{E} = -\,\mathrm{grad}\,V$

$\mathcal{E}_x = -dV/dx = -2U/a^2\,x$

$\mathcal{E}_y = -dV/dy = 2U/a^2\,y$

$F_x = -2\,Uqe/a^2\,x$

$F_y = 2\,Uqe/a^2\,y$

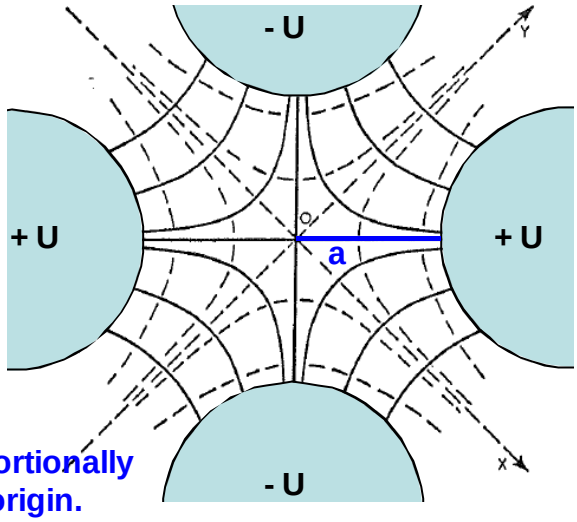

1. Force increases proportionally to distance from origin.
2. Focusing in x and defocusing in y (or vice versa).

$\Rightarrow$ requires quadrupole doublet or triplet to focus in x and y

Multipole correction elements

Correction of higher-order effects (aberrations) by hexapole, octupole, etc. fields. Often limited by beam diagnostics!

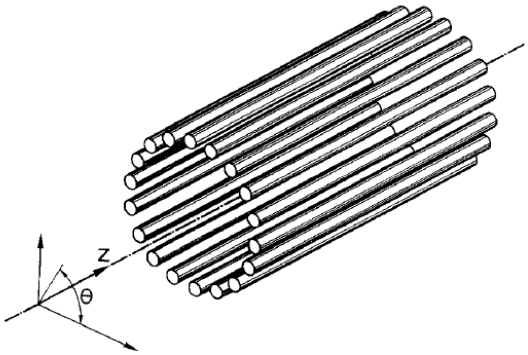

Fig. 1. Squirrel-cage-like electrode arrangement of an electrostatic $2(n+1)$ pole consisting of 18 wires, i.e. a squirrel-cage with $n=8$. In this multipole the potential of each wire is controlled by a separate power supply.

Fig. 3. Calculated potential distributions in a 32-wire squirrel-cage multipole for the cases of dipole ($V_1 \neq 0$), quadrupole ($V_2 \neq 0$), hexapole ($V_3 \neq 0$), octupole ($V_4 \neq 0$) excitations [see eq. (1)] with vanishing ψ_1, ψ_2, ψ_3, ψ_4.

M. Antl and H. Wollnik, Nucl. Instr. Meth. A274 (1989) 45.

Ion-optical calculations

1. Matrix calculation:

TRANSPORT, COSY-INFINITY, GIOS, GICO, LISE++,...

2. MC simulations/ray tracing:

SIMION, ZGOUBY, RAYTRACE, LISE++, MOCADI,...

Focal plane of LOHENGRIN

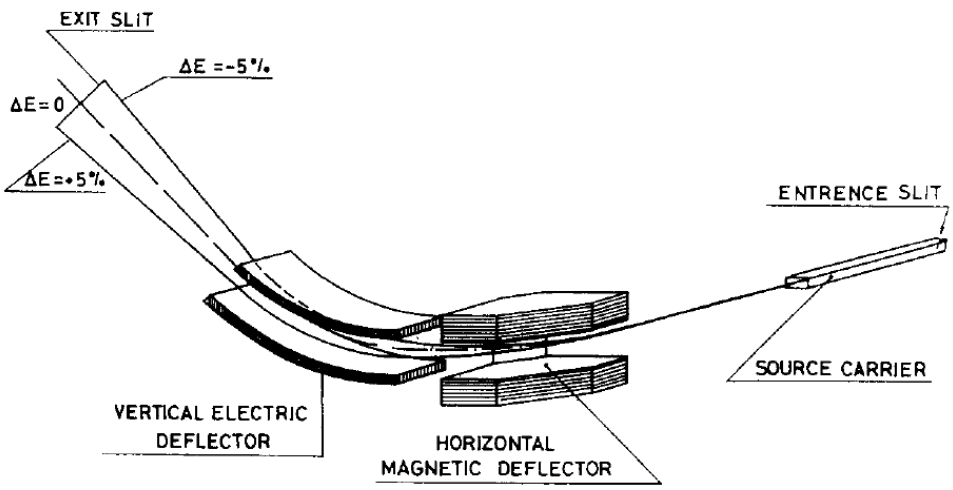

P. Armbruster et al., Nucl. Instr. Meth. 139 (1976) 213.

LOHENGRIN focal plane

Energy dispersion: $\Delta x = D_E \, \Delta E/E = 7.2$ cm/% $= 7.2$ m

Mass dispersion: $\Delta y = D_m \, \Delta m/m = 3.24$ cm/% $= 3.24$ m

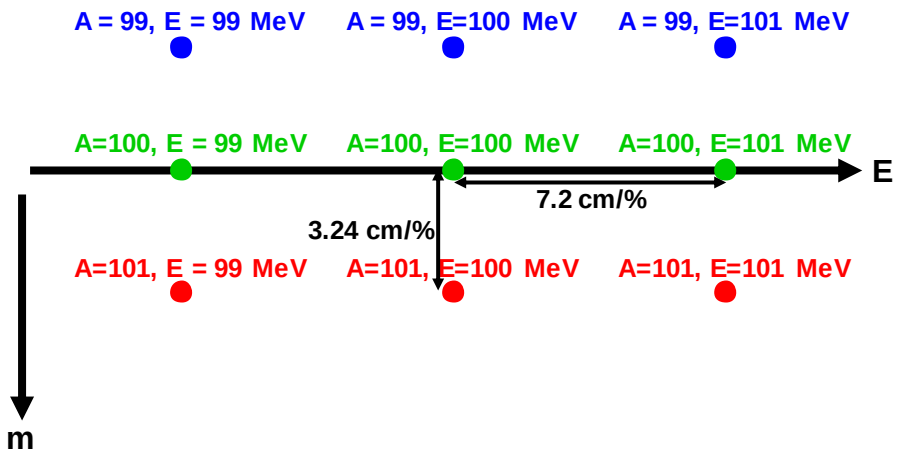

LOHENGRIN energy resolution

Magnification in x: $x_i = M_x\, x_o$

Energy resolution: $R_E = x_i / D_E = M_x \cdot x_o / D_E =$

$= 1.0 \cdot 7.0\ \text{cm} / 7.2\ \text{m} \approx 1/100$

depends on target length!

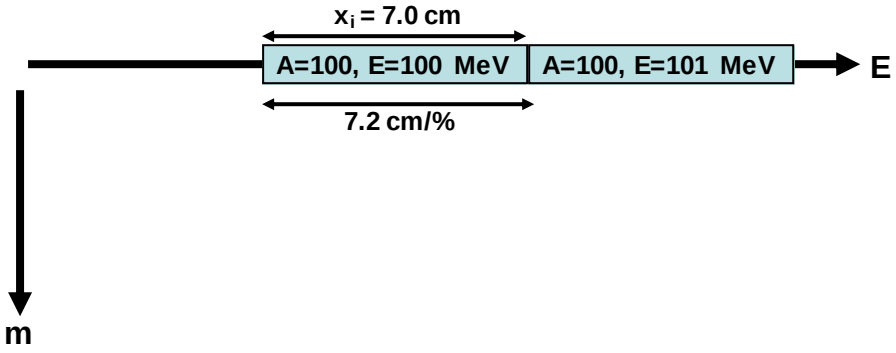

LOHENGRIN mass resolution

Magnification in y: $y_i = M_y\, y_o$

Mass resolution: $R_m = y_i / D_m = M_y \cdot y_o / D_m =$

$= 1.0 \cdot 0.3\ \text{cm} / 3.24\ \text{m} \approx 1/1000$

depends on target width!

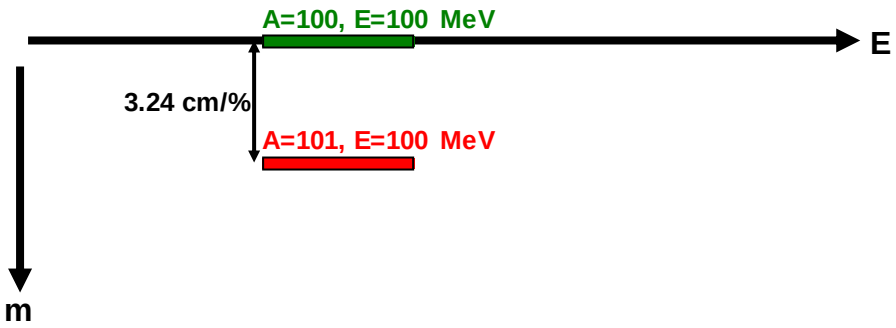

A/q separator

A "mass" separator is in reality an A/q separator and will mix masses with the same A/q and same E/q.

Avoid the use of A/q with (near-)integer ratios!

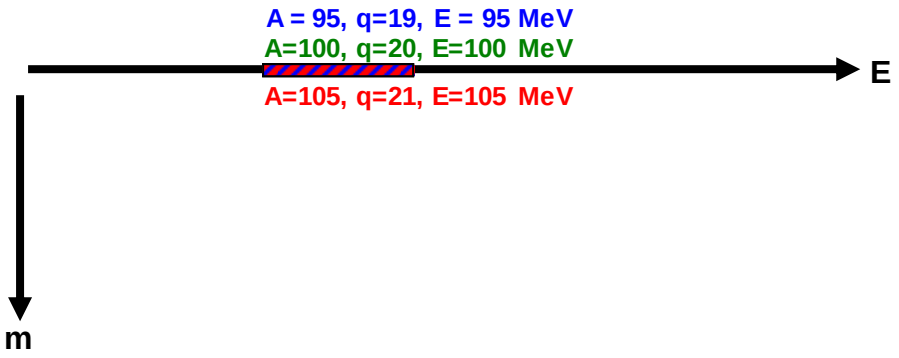

Focal plane of LOHENGRIN

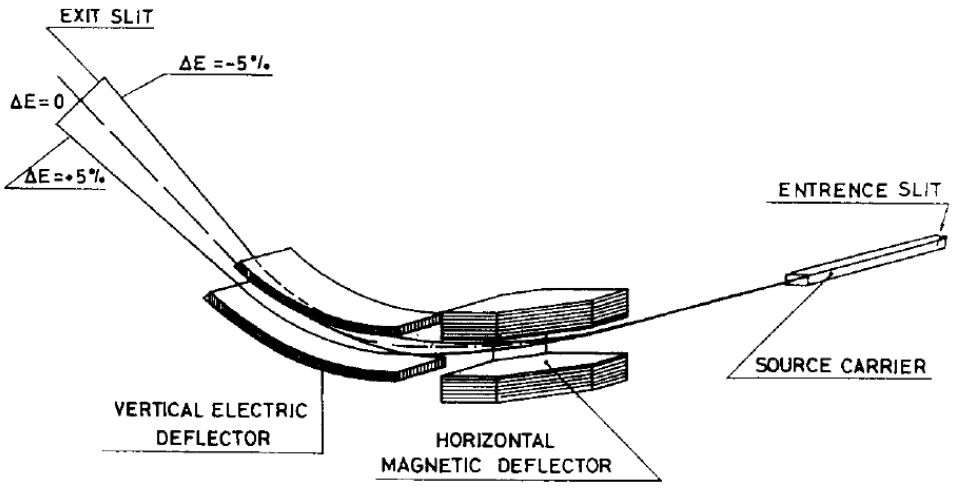

Measured kinetic energy distribution

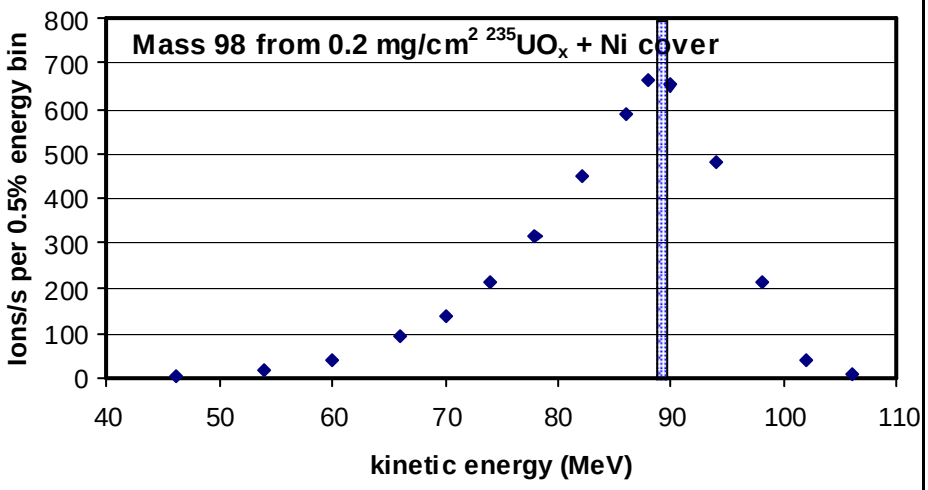

kinetic energy acceptance: ΔE/E = 1%

Reverse Energy Dispersion magnet

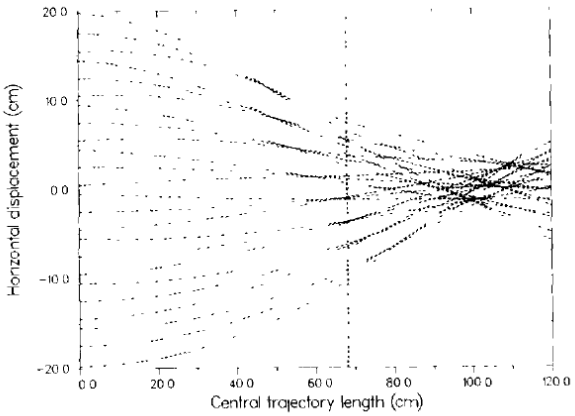

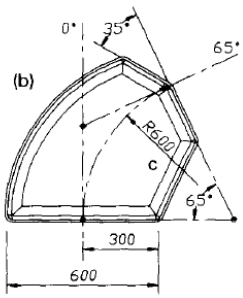

Fig. 5. Horizontal displacement with respect to the central trajectory of a beam arising from a 5×70 mm^2 target vs the central trajectory length. The vertical dashed and dotted lines show respectively the extent of the pole pieces and the focal position.

G. Fioni et al., Nucl. Instr. Meth. A332 (2003) 175.

LOHENGRIN Setup

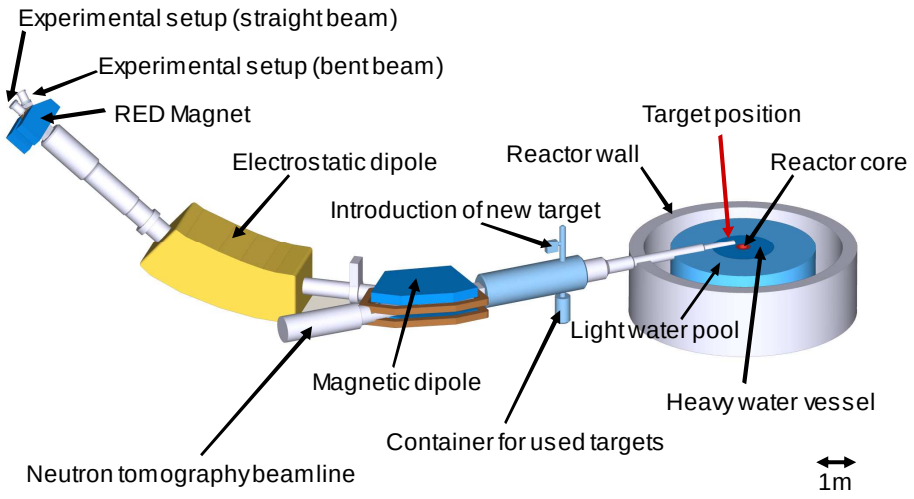

Measured kinetic energy distribution

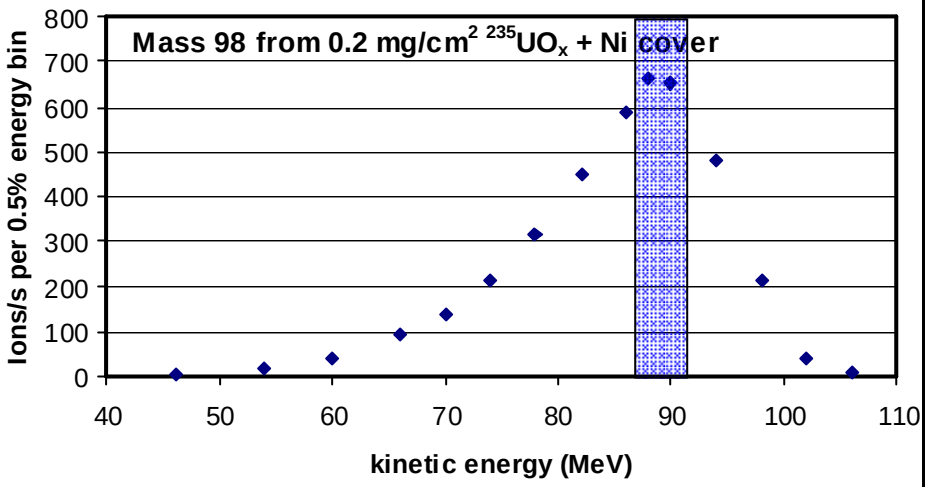

kinetic energy acceptance: ΔE/E = 5%

⇒ 10-60% transmission (low for thick spectroscopy targets)

Detection of rare ternary particles

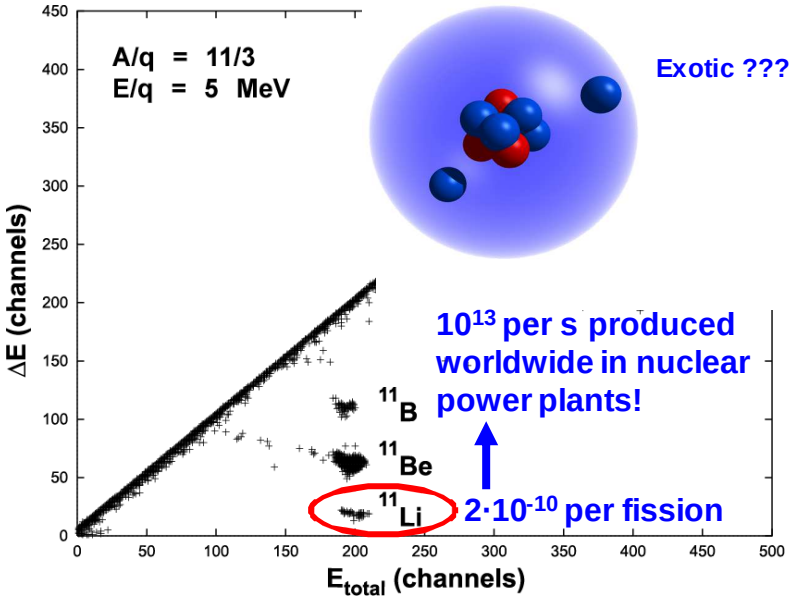

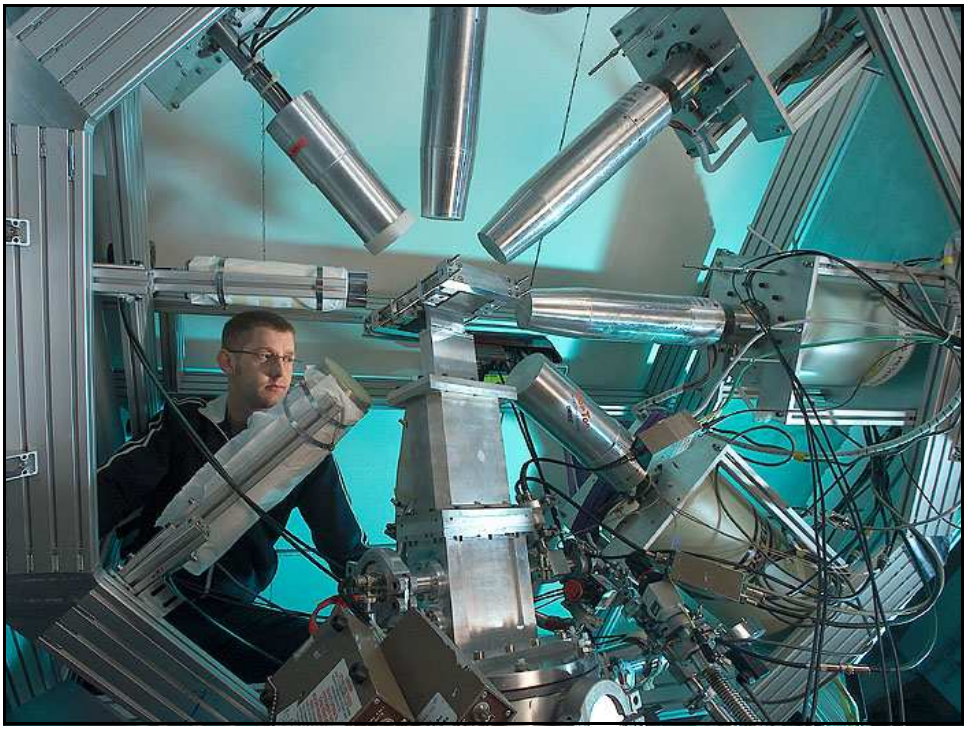

Gamma decay of 7.6 μs ^{98}Y isomer

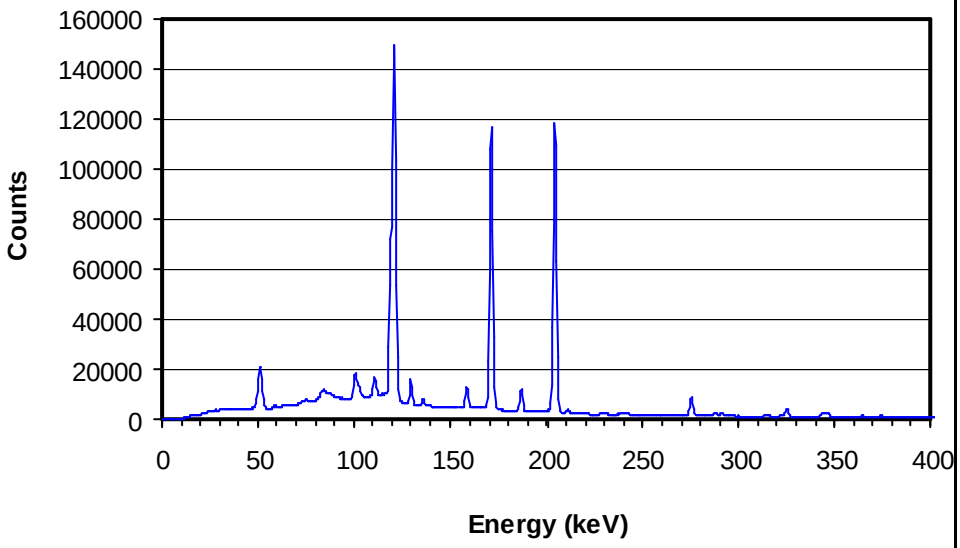

17$^-$ isomer at 6.6 MeV in ^{98}Zr

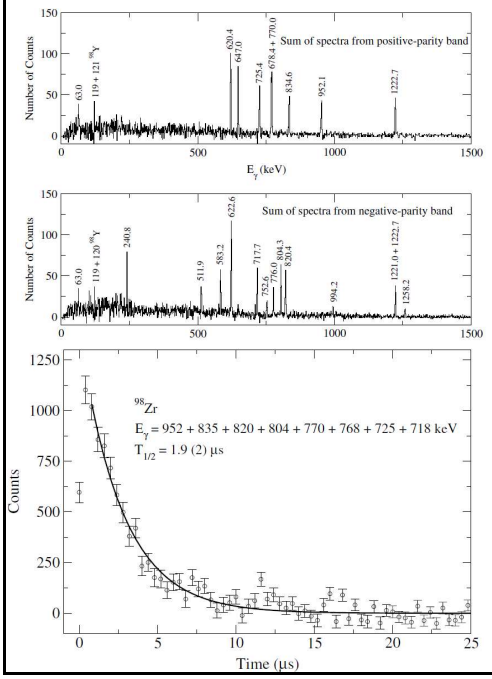

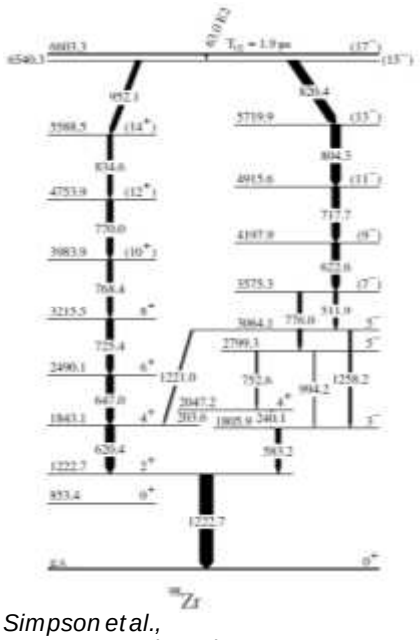

G. Simpson et al., Phys. Rev. C 74 (2006) 064308.

Existing thick-target ISOL beams

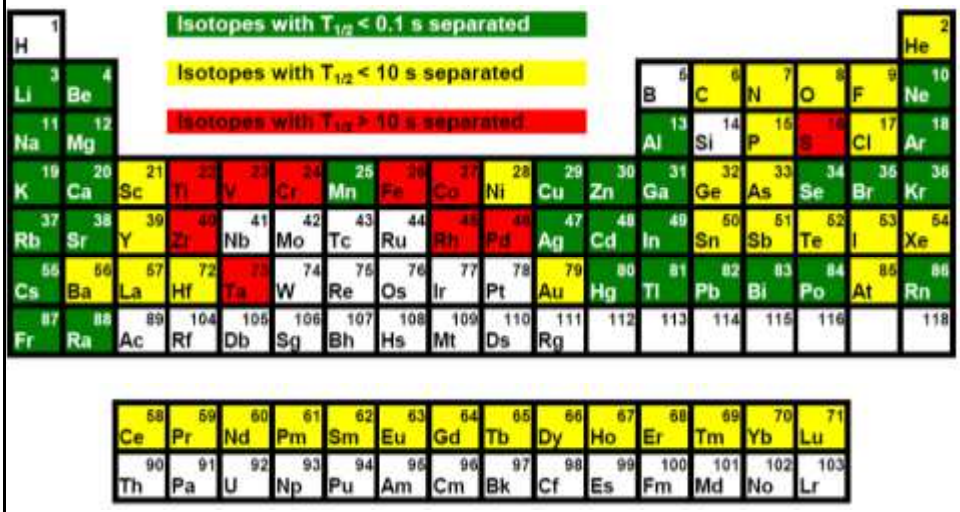

The LOHENGRIN fission fragment separator

mass-separated fission fragments,

up to 10^5 per second, $T_{1/2} \geq$ microsec.

$\Delta A/A$ = 3E-4 – 3E-3

$\Delta E/E$ = 1E-3 – 1E-2

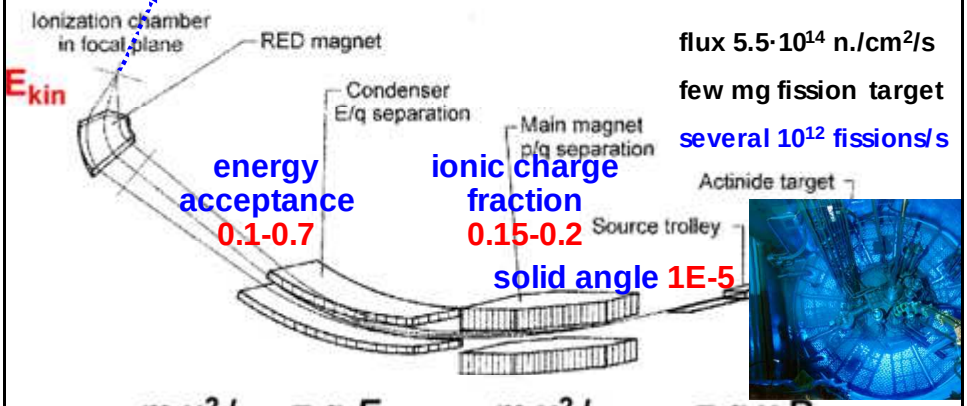

flux 5.5·10^{14} n./cm²/s

few mg fission target

several 10^{12} fissions/s

$m v^2 / r_{el} = q E$ $\quad E_{kin} / q = E / 2 r_{el}$

$m v^2 / r_{magn} = q v B$ $\quad m v / q = B r_{magn}$

Ionic charge separation

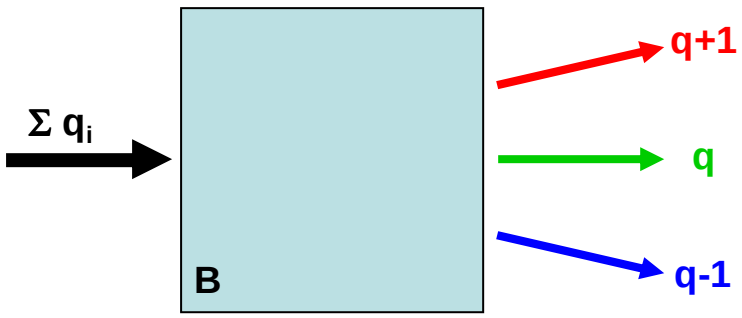

Ionic charge state distribution

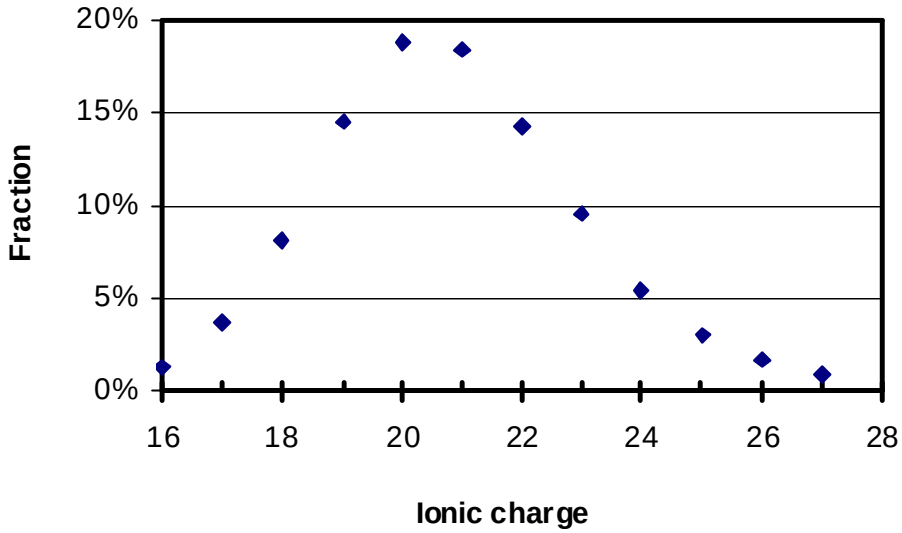

Ionic charge separation

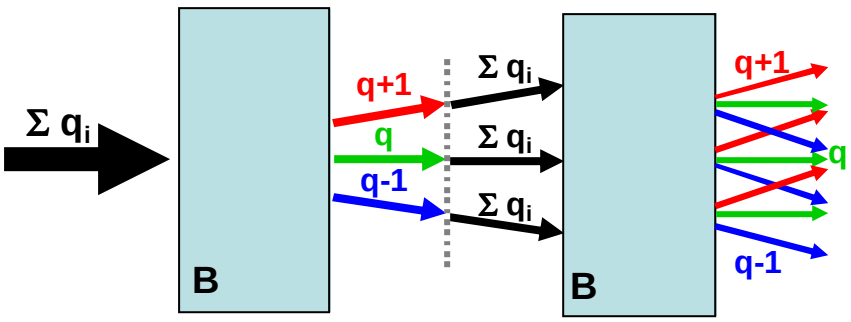

Ionic charge separation

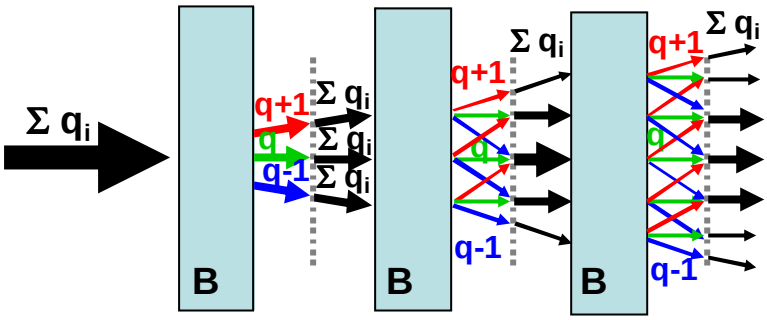

Separation with gas-filled magnet

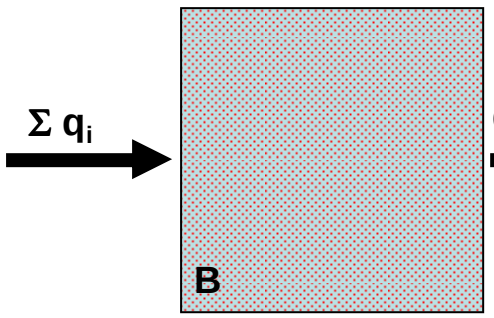

He or N_2 at few mbar

$q_{average} = v/v_{Bohr}\ Z^{\alpha}$

$\alpha_{theo} = 1/3$ (Bohr)

$\alpha_{exp} = 0.33 - 0.7$

Isotope selection with gas-filled separators

- Gas collisions give average $q = fkt(Z,v) \propto Z^{1/3}\ v/v_{Bohr}$
- p/q selection by magnetic deflection
- $B\rho \propto A/Z^{1/3}$ (*A. Ghiorso et al., Nucl. Instr. Meth. A269 (1988) 192*)

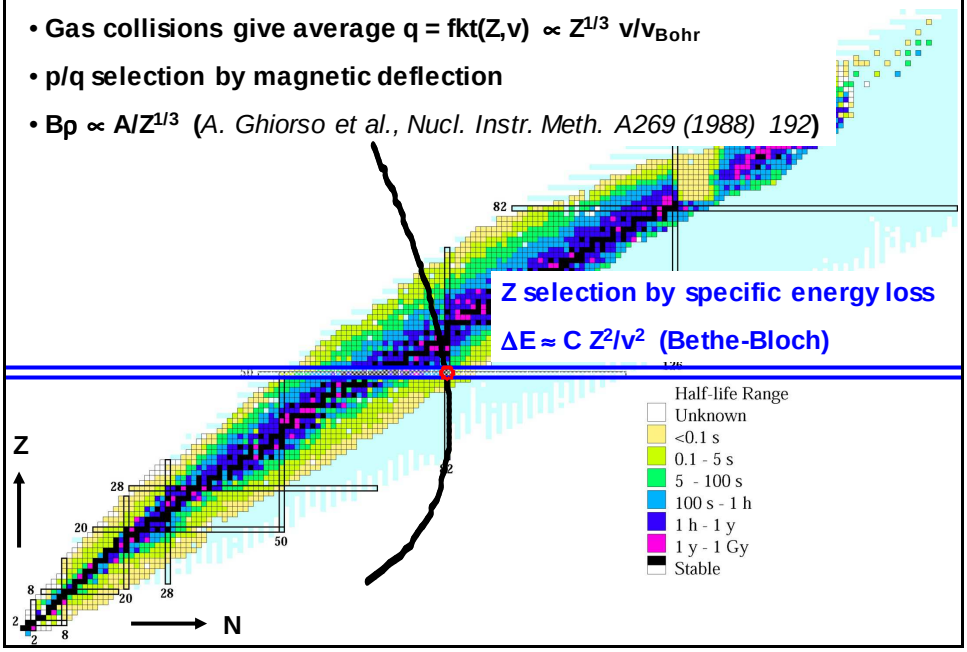

Multistep-Separation in Accelerator Mass Spectrometry

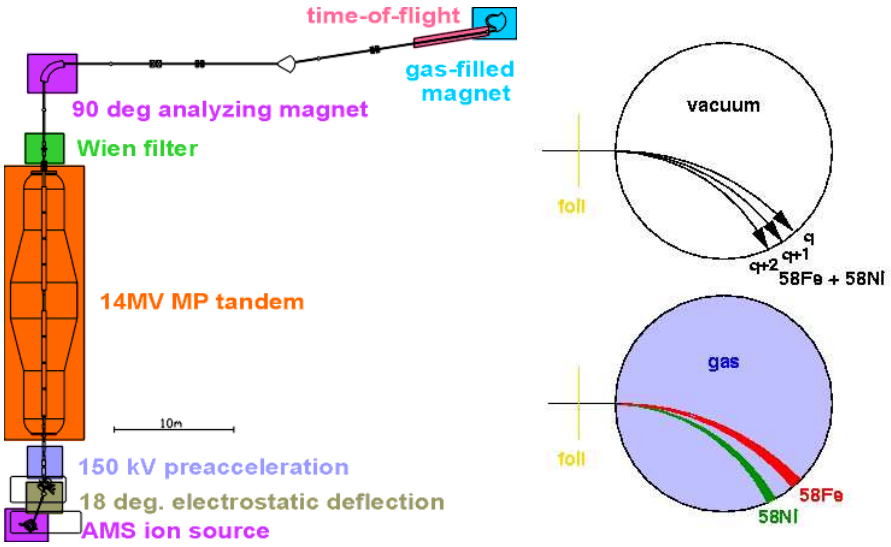

10^{-15} sensitivity!

From ISOL beams to RIBs with higher energies

ISOL beams

- **have well-defined energy ($\Delta E/E \approx$ 1eV / 60 keV)**
- **have usually small emittance (e.g. 10 π mm mrad), i.e. limited opening angle**
- **have often well-defined ionic charge q=1**
- **Z selection is performed before the mass separator**

Recoils or fragments of nuclear reactions:

- **have large energy spread**
- **large angular spread**
- **different ionic charge states**
- **depending on nuclear reaction different Z**

Fusion-evaporation

$^{58}Ni(^{58}Ni,2n)^{114}Ba$

$^{58}Ni(^{58}Ni,\alpha 2n)^{110}Xe$

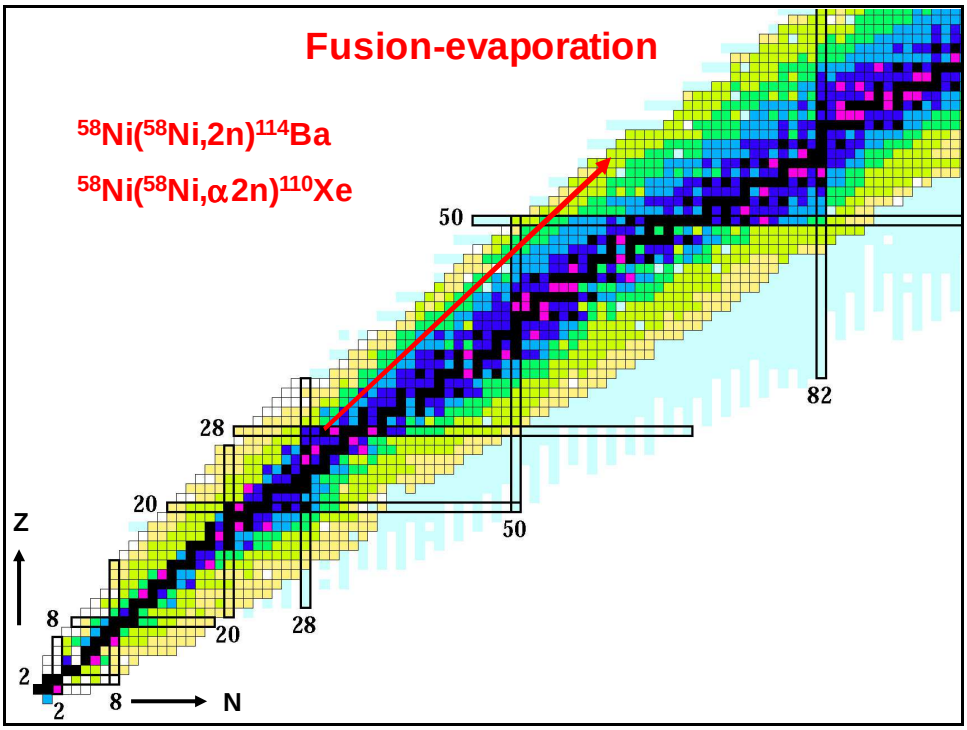

Multinucleon transfer reactions

$^{186}W(^{64}Ni,X)^{184}Lu$

K. Krumbholz et al.,

Z. Phys. A352 (1995) 1.

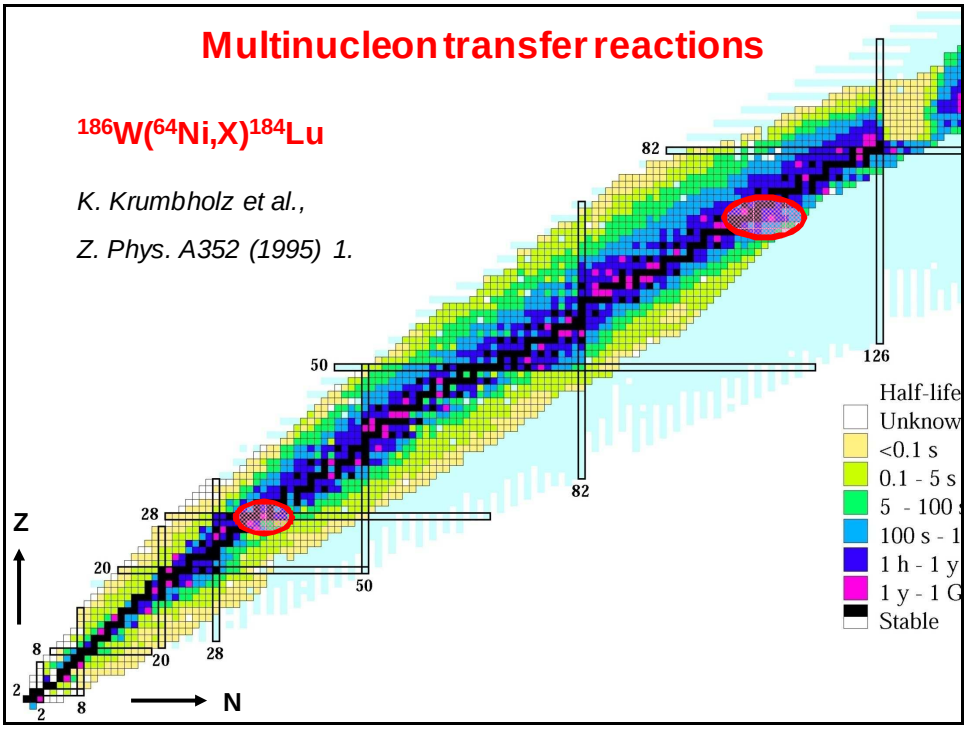

Requirements for in-flight separators

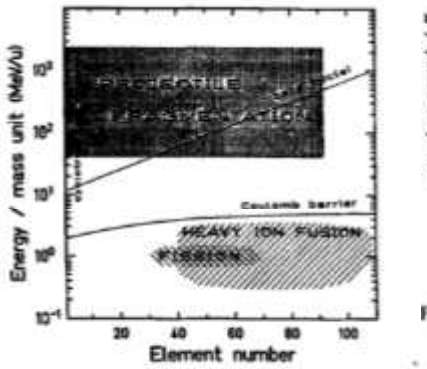

Fig. 2. Domains of kinetic energies of the reaction products from various nuclear reactions.

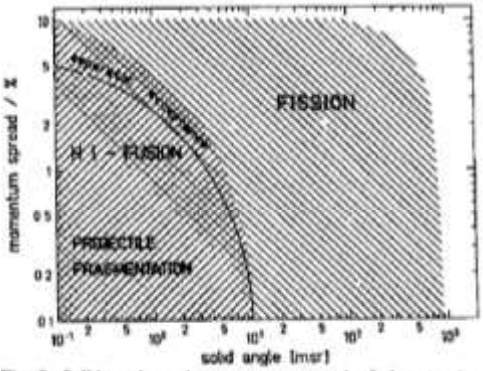

Fig. 3. Solid angle and momentum spread of the reaction products compared to the acceptances of spectrometers.

G. Münzenberg, Nucl. Instr. Meth. B70 (1992) 265.

Recoil separators

- separate the products of a nuclear reaction (recoils) from the projectile beam
- early dumping of unwanted beam
- optionally also A/q separation of reaction products
- usually kinetic energies up to 10 MeV/nucleon
- mass dispersion achieved by combination of magnetic dipoles, electric dipoles or Wien filter
- usually additional quadrupoles for focusing

SHIP at GSI Darmstadt

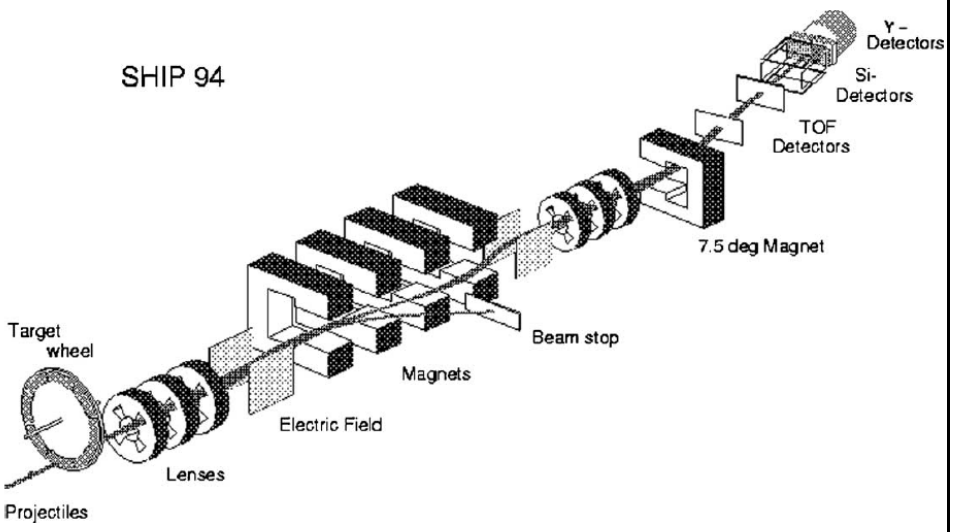

G. Münzenberg et al., Nucl. Instr. Meth. 161 (1979) 65.

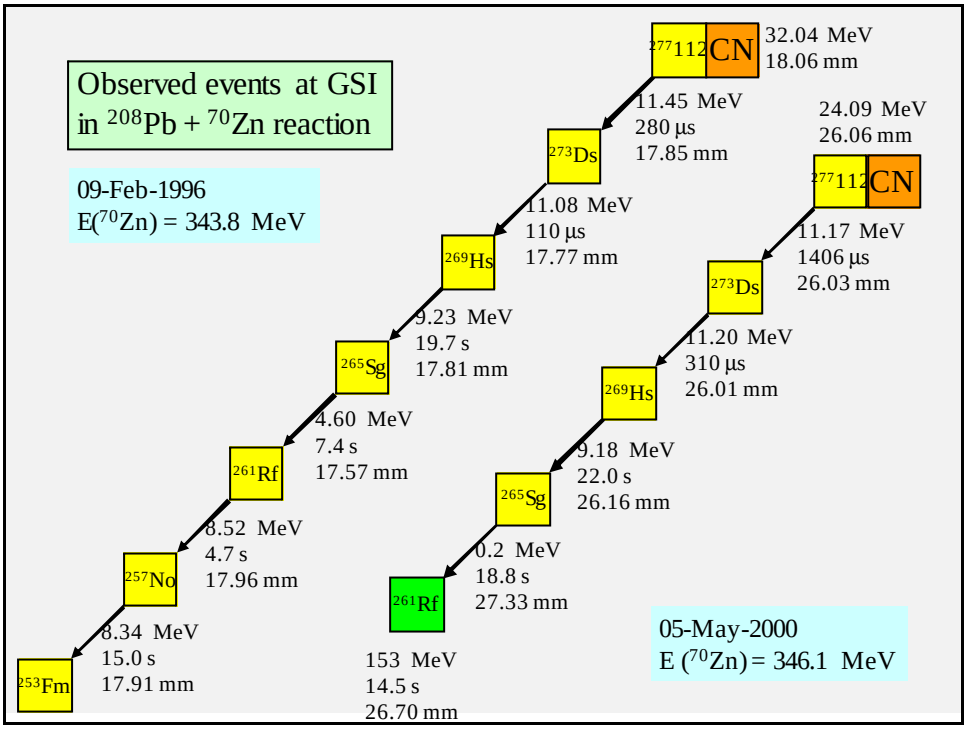

VASSILISSA

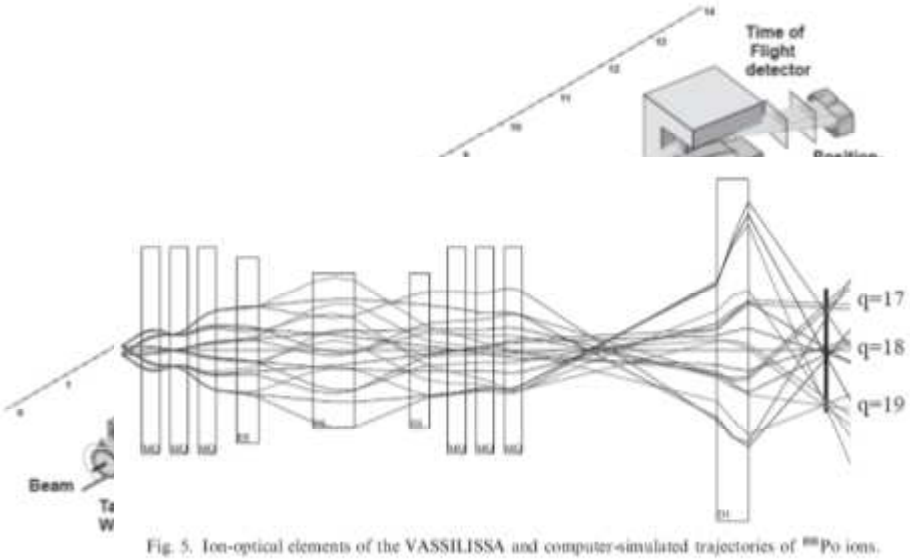

Fig. 5. Ion-optical elements of the VASSILISSA and computer-simulated trajectories of ^{208}Po ions.

A.G. Popeko et al., Nucl. Instr. Meth. A510 (2003) 371.

DGFRS: Dubna Gas-Filled Recoil Separator

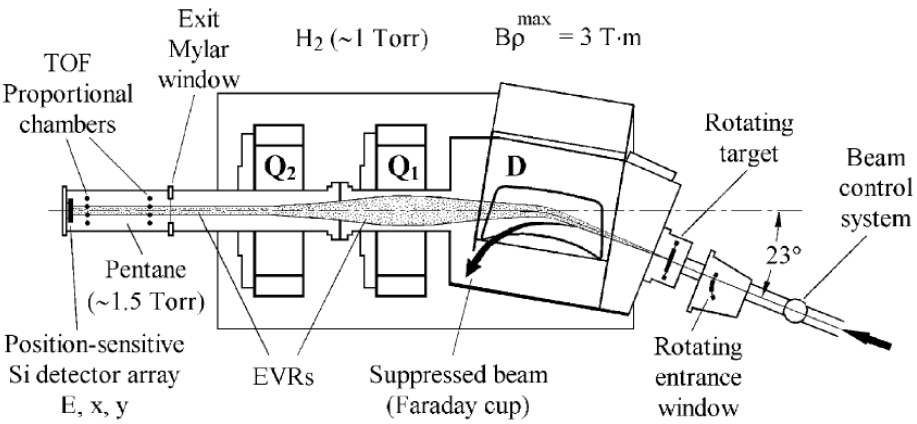

K. Subotic et al., Nucl. Instr. Meth. A481 (2002) 71.

RIKEN Gas-filled Recoil Separator GARIS

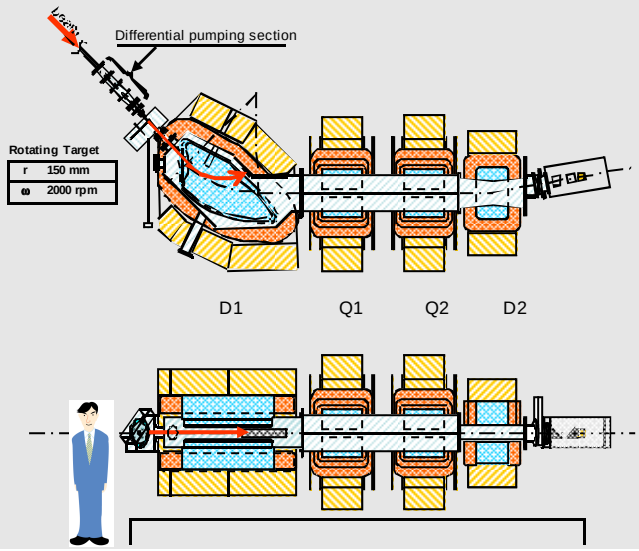

D1	
Bending angle	45 degree
Pole gap	150 mm
Radius of central ray	1200 mm
Maximum field	1.54 T

Q1, Q2	
Pole length	500 mm
Bore radius	150 mm
Maximum field gradient	5.2 T/m

D2	
Bending angle	10 degree
Pole gap	160 mm
Pole length	400 mm
Maximum Field	1.04 T

Magnification	X	-0.76
	Y	-1.99
Dispersion		0.97 cm/%
Total length		5760 mm
Acceptance	Δθ	± 68 mrad
	Δφ	± 57 mrad
	ΔΩ	12.2 msr

Decay chains from $^{48}Ca + ^{238}U \Rightarrow ^{286}112^*$

DGFRS mean values

$^{283}112$ CN

α_1: $E_\alpha = 9.54 \pm 0.06$ MeV, $T_{1/2} = 3.8$ s, $b_{sf} \le 0.10$ → ^{279}Ds

α_2: 9.70 / 228 MeV, $T_{1/2} = 0.20$ s, $b_\alpha = 0.10$ → ^{275}Hs

α_3: 9.30 MeV, $T_{1/2} = 0.19$ s, $b_\alpha = 1.0$ → ^{271}Sg

α_4: 8.54 / 248 MeV, $T_{1/2} = 1.9$ min, $b_\alpha = 0.70$ → ^{267}Rf

260 MeV TKE, $T_{1/2} = 1.3$ h, $b_{sf} = 1.0$

$\sigma = (2.5^{+1.8}_{-1.1})$ pb (DGFRS)

$\sigma = (1.0^{+1.0}_{-0.6})$ pb (SHIP, $^{238}U_{metal}$)

$\sigma = (0.7^{+0.6}_{-0.4})$ pb (SHIP, $U_{met} + UF_4$)

Yu.Ts. Oganessian et al., Phys. Rev. C74, 44602 (2006)

SHIP mean values

$^{283}112$ CN

α: 9.520 ± 0.015 / 232 ± 15 MeV, $T_{1/2} = 6.9^{+6.9}_{-2.3}$ s, $b_{sf} = 0.5$ → ^{279}Ds

210^{+30}_{-15} MeV, $T_{1/2} = 0.18^{+0.32}_{-0.07}$ s

S. Hofmann et al., Eur. Phys. J. A32, 251 (2007)

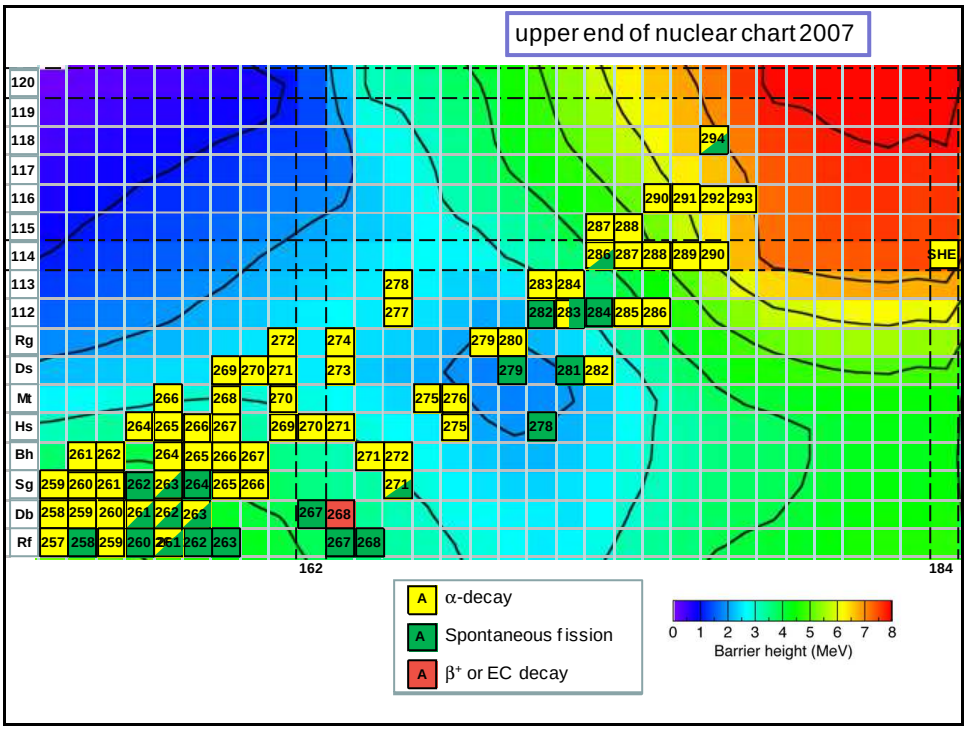
upper end of nuclear chart 2007
120
119
118
117
116
115
114
113
112
Rg
Ds
Mt
Hs
Bh
Sg
Db
Rf
162
184
SHE
A α-decay
A Spontaneous fission
A β+ or EC decay
0 1 2 3 4 5 6 7 8
Barrier height (MeV)

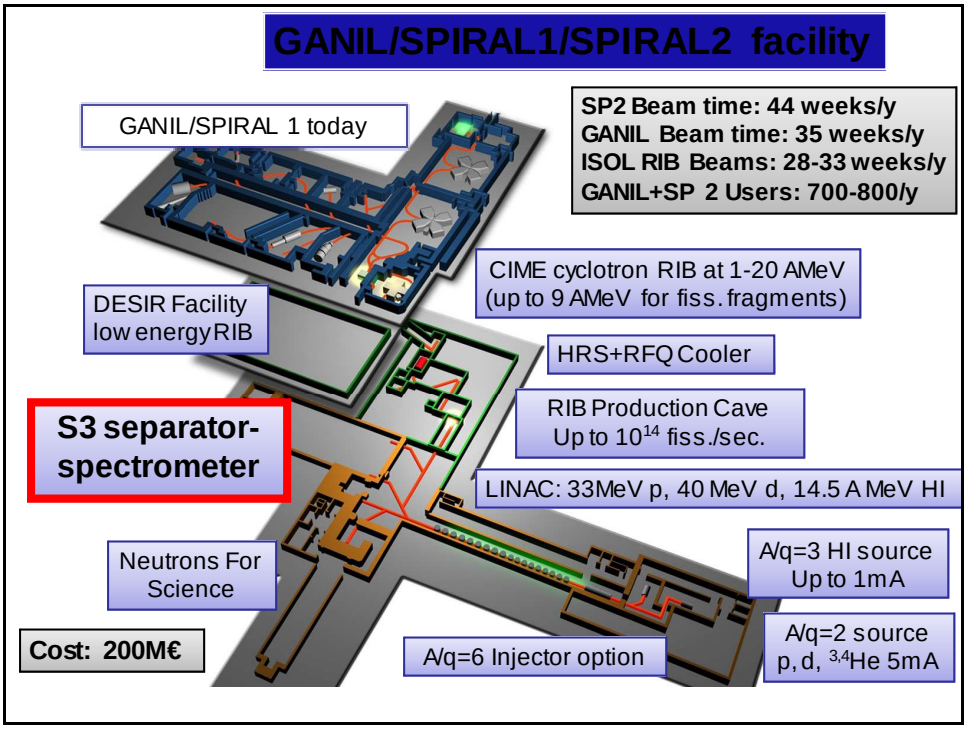
GANIL/SPIRAL1/SPIRAL2 facility
GANIL/SPIRAL 1 today
SP2 Beam time: 44 weeks/y
GANIL Beam time: 35 weeks/y
ISOL RIB Beams: 28-33 weeks/y
GANIL+SP 2 Users: 700-800/y
CIME cyclotron RIB at 1-20 AMeV
(up to 9 AMeV for fiss. fragments)
DESIR Facility
low energy RIB
HRS+RFQ Cooler
S3 separator-
spectrometer
RIB Production Cave
Up to 10^14 fiss./sec.
LINAC: 33MeV p, 40 MeV d, 14.5 A MeV HI
Neutrons For
Science
A/q=3 HI source
Up to 1mA
Cost: 200M€
A/q=6 Injector option
A/q=2 source
p, d, 3,4He 5mA

S3 at SPIRAL2, GANIL, Caen

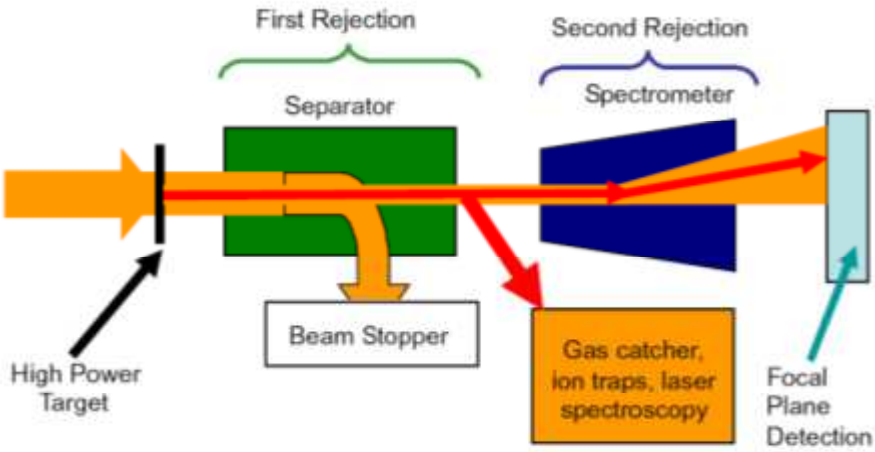

Fig. 1. Schematic idea for S^3 showing the two stage separator.

S3 at SPIRAL2, GANIL, Caen

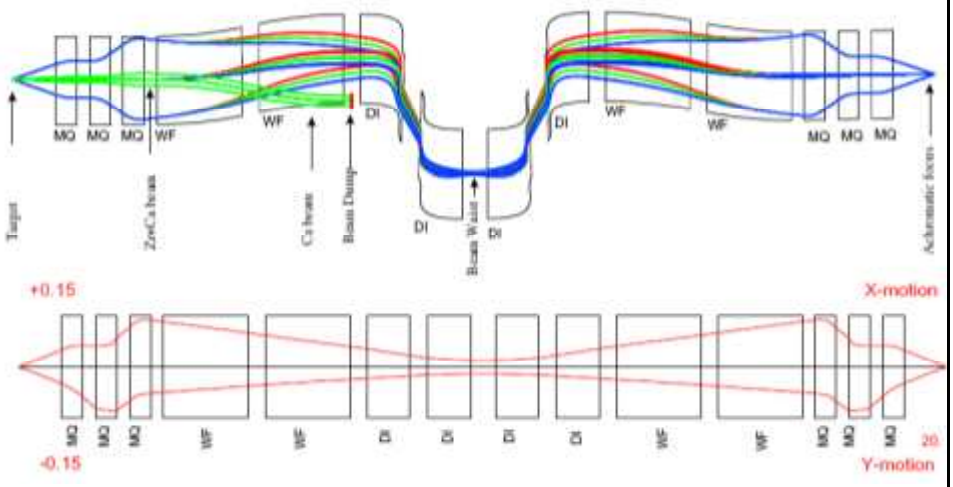

A. Drouart et al., Nucl. Instr. Meth. B266(2008) 4162.

VAMOS at GANIL

Very wide acceptance ⇒ trajectory reconstruction for aberration correction

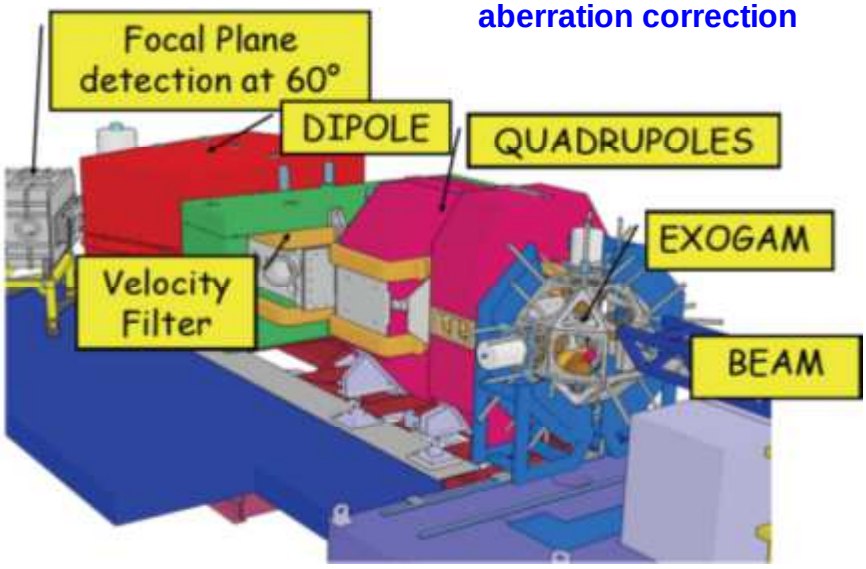

H. Savajols for the VAMOS Collaboration, Nucl. Instr. Meth. B204 (2003) 146.

DRAGON

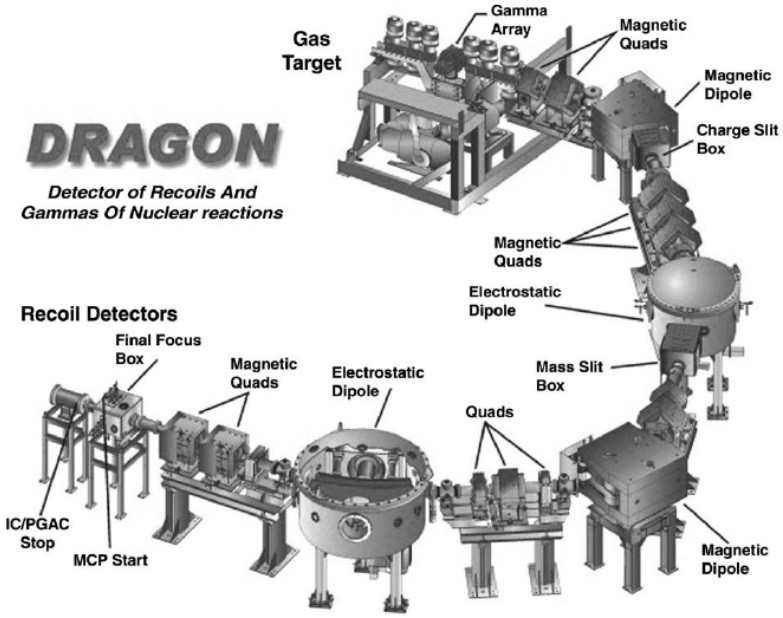

D. Hutcheon, Nucl. Instr. Meth. A498 (2003) 190.

Spallation + Fragmentation + Fission

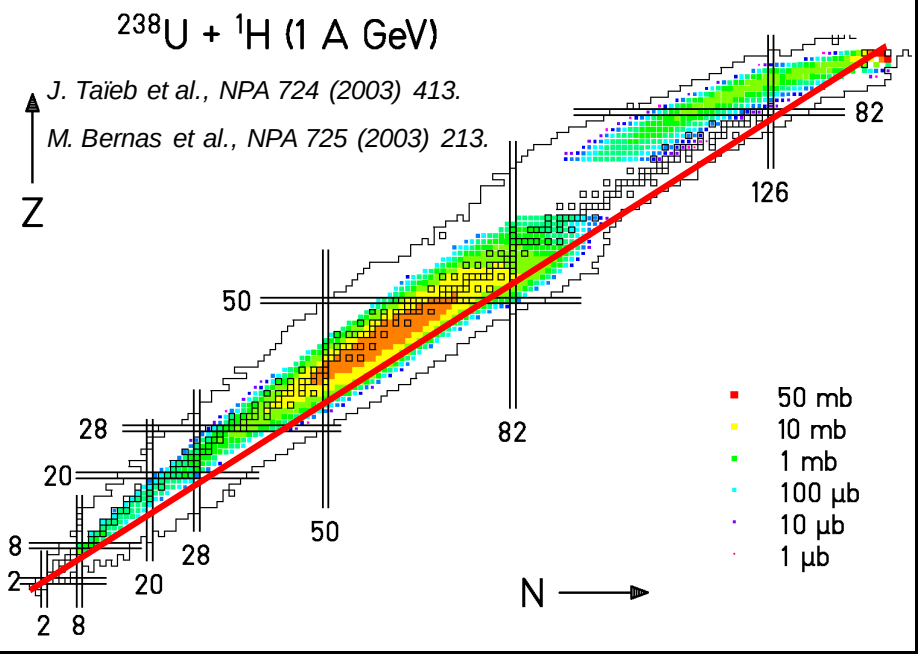

Normal kinematics: n, p or light ions on heavy target

- "conventional" accelerator providing "easily" high beam intensity
- dedicated target required
- reaction products emitted into 4π

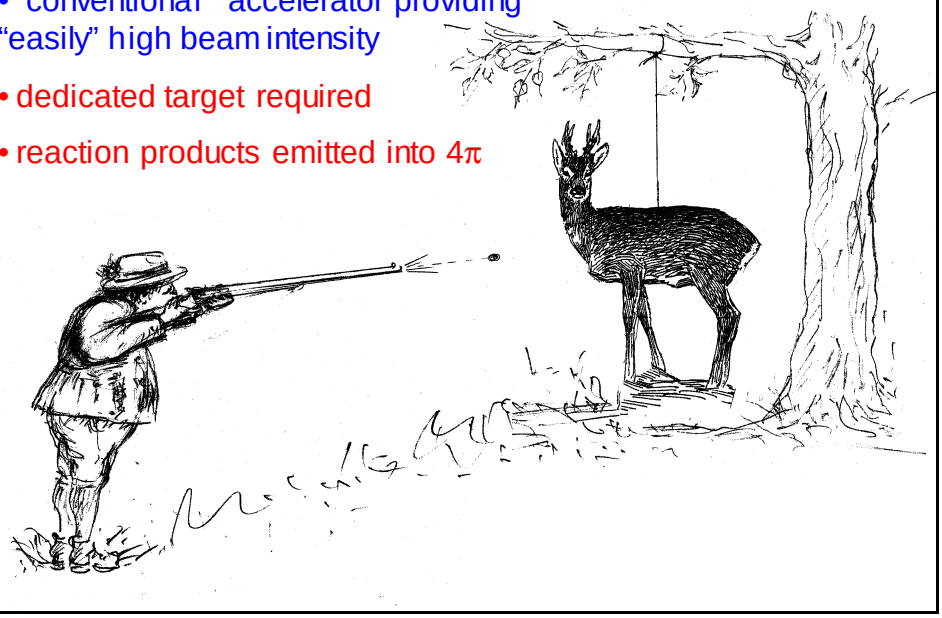

Inverse kinematics: heavy ions on light target

- complex and expensive accelerator
- reaction products forward focused

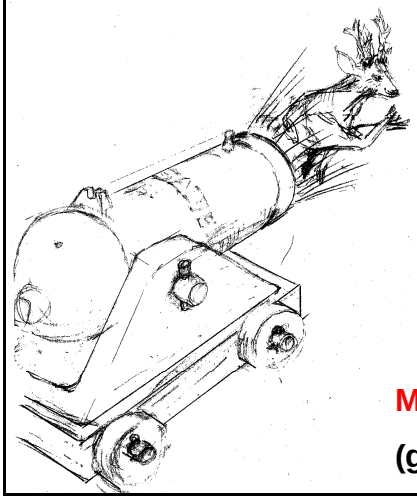

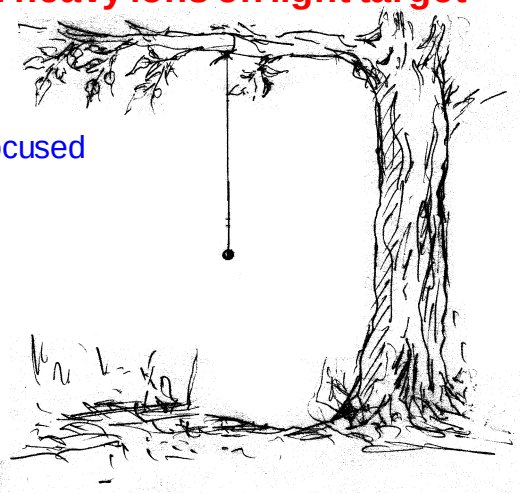

Mind the losses during stopping!

(graphical representation censored)

Spallation + Fragmentation + Fission

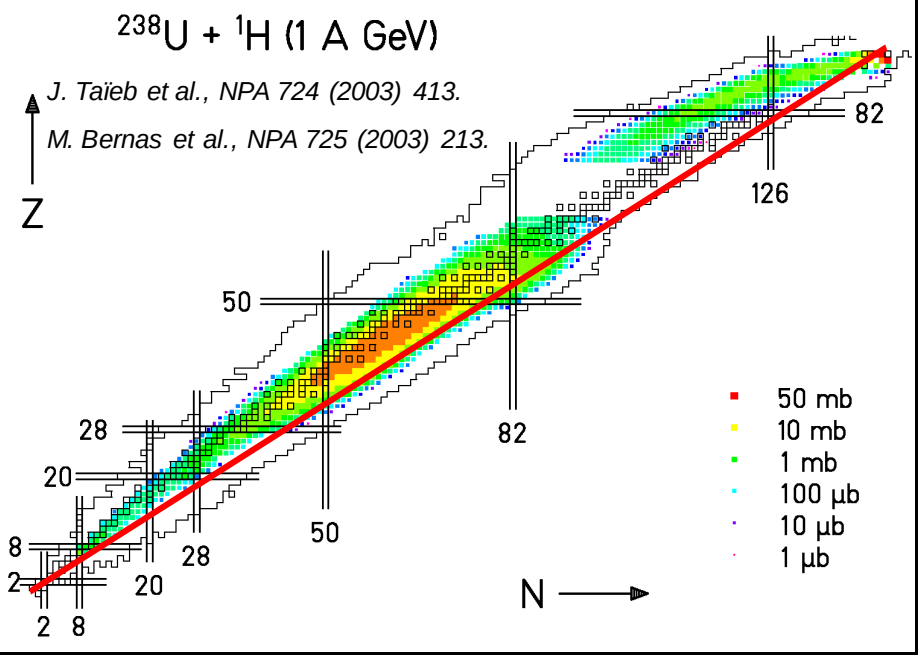

Momentum-loss achromat (Wedge separation)

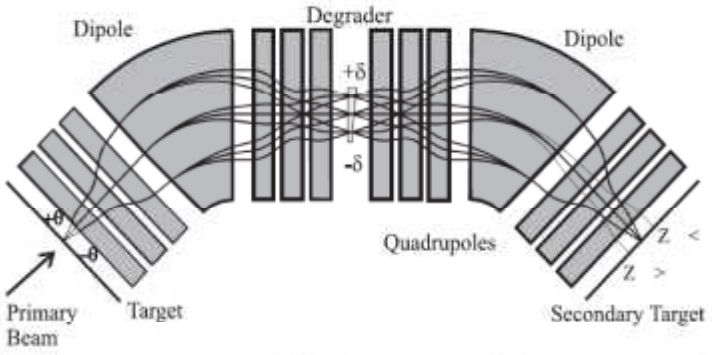

Fig. 4. Schematic representation of the ion-optics used in a momentum-loss achromat to separate projectile fragments.

D.J. Morrissey and B.M. Sherill, Lecture Notes in Physics 651 (2004) 113.

LISE

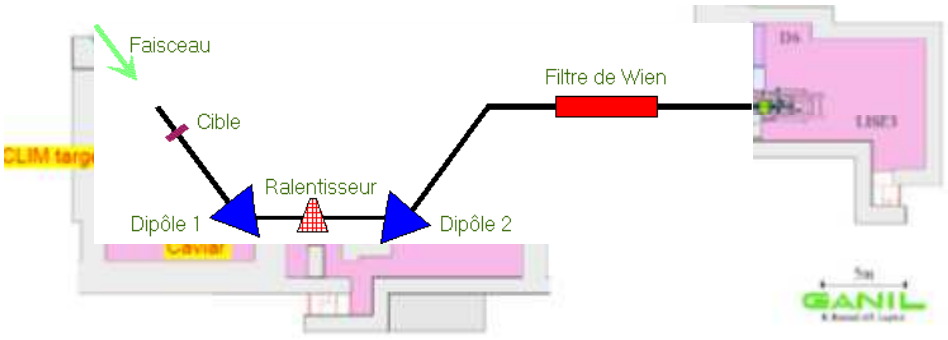

R. Anne et al., Nucl. Instr. Meth. A257 (1987) 215.
R. Anne et al., Nucl. Instr. Meth. B70 (1992) 276.

Dispersive ion optical elements

- magnets are momentum dispersive
- electrostatic deflectors are energy dispersive
- Wien filters are velocity dispersive
- achromatic wedges are dispersive in mZ^2/E or $(Z/v)^2$
- RF kicker are flight time selective

Effect of wedge selection

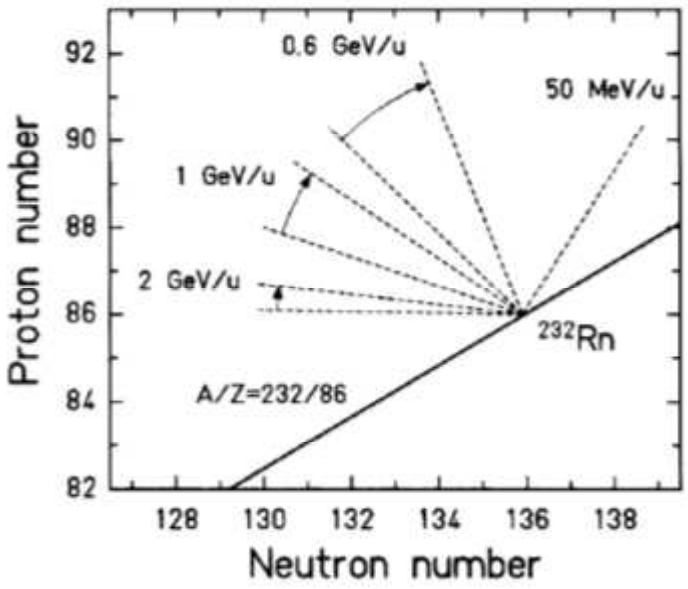

K.H. Schmidt et al., Nucl. Instr. Meth. A260 (1987) 287.

Effect of wedge selection

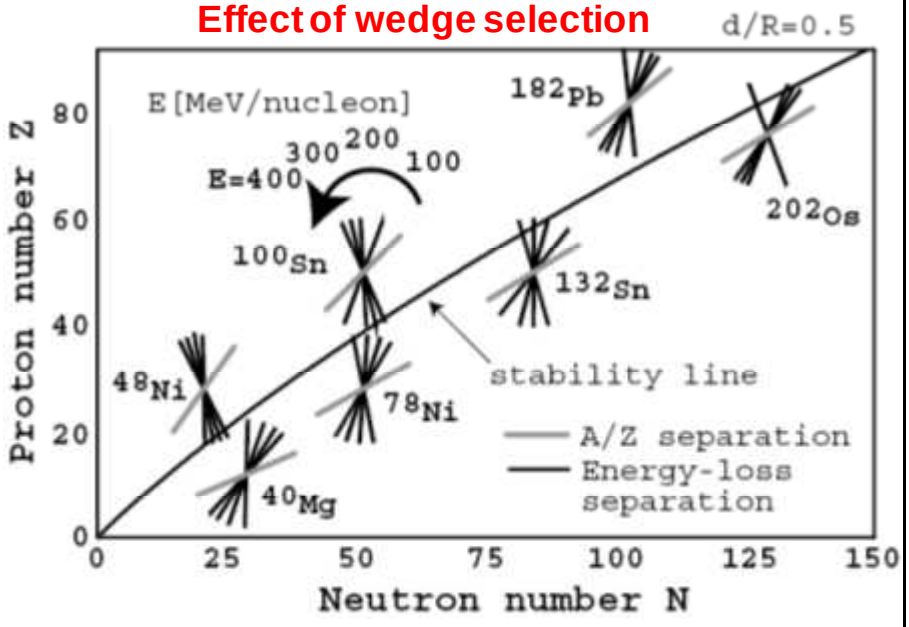

T. Kubo, Nucl. Instr. Meth. B204 (2003) 97.

In-flight production of rare isotopes

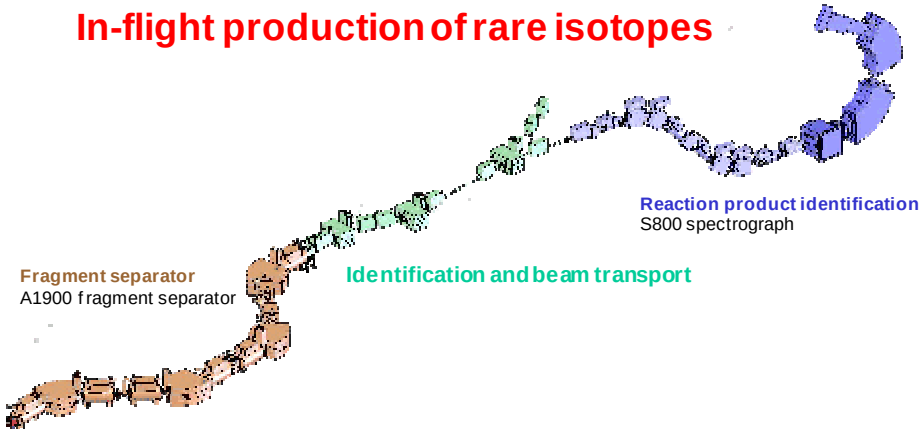

Driver accelerator (v = 0.25-0.6 c)

- **Fragment separator (A1900 NSCL, FRS GSI, BigRIPS RIKEN, ALPHA spectrometer/LISE GANIL)**
- **Identification and beam transport**
  - Stopped beam experiments, reaccelerated beam experiments
  - Fast beam experiments
    - Secondary reaction
    - Reaction product identification (S800 spectrograph, CATE/Aladin, Silicon telescopes/TOF wall, SPEG)

In-flight production of rare isotopes

Example: ^{78}Ni from ^{86}Kr at NSCL

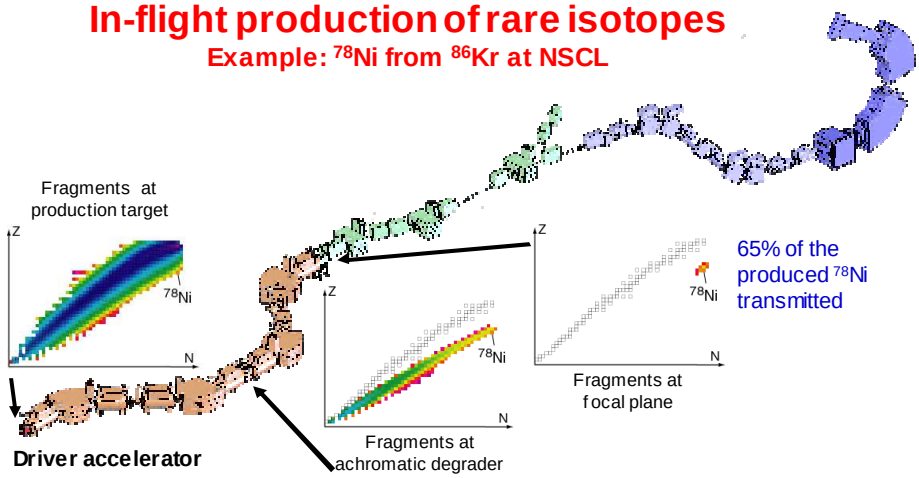

- **Fragment separator** (**A1900** NSCL, **FRS** GSI, **BigRIPS** RIKEN, **ALPHA/LISE** GANIL)
- **Identification and beam transport**
  - Stopped beam experiments
  - Fast beam experiments
    - Secondary reaction
    - Reaction product identification (S800 spectrograph, CATE/Aladin, Silicon telescopes/TOF w all, SPEG)

Isotope selection at (high E) in-flight separators

- **Ionization to q = Z (high energies!)**
- **A/Z selection by magnetic deflection**
- **Bρ ∝ A/Z v γ**
- **v can be measured by time of flight or selected by Wien filter**

Z selection by specific energy loss

$\Delta E \approx C\, Z^2/v^2$ (Bethe-Bloch)

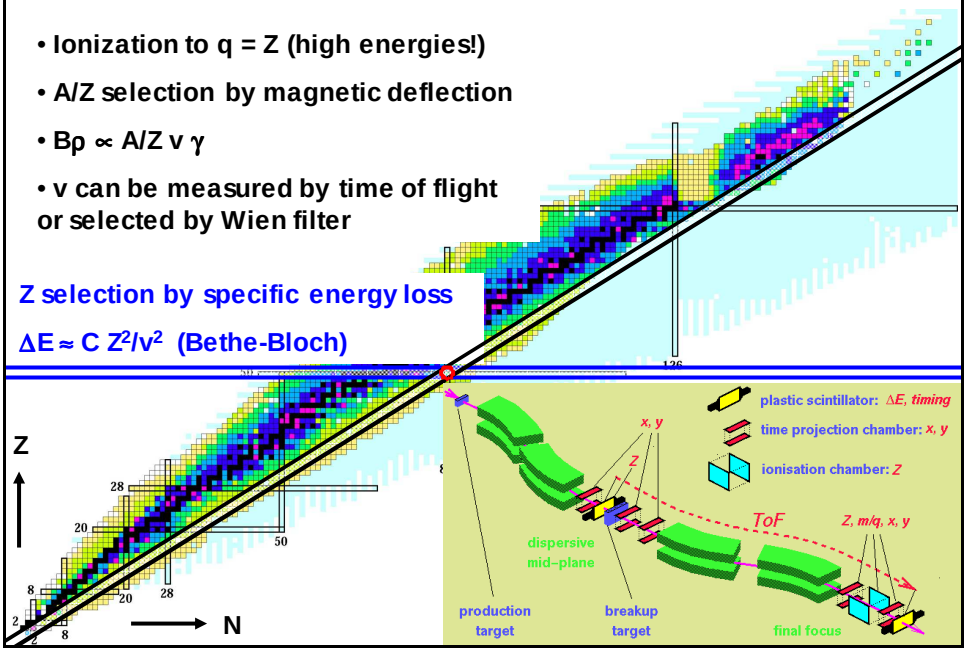

Perfect isotope identification at high energy

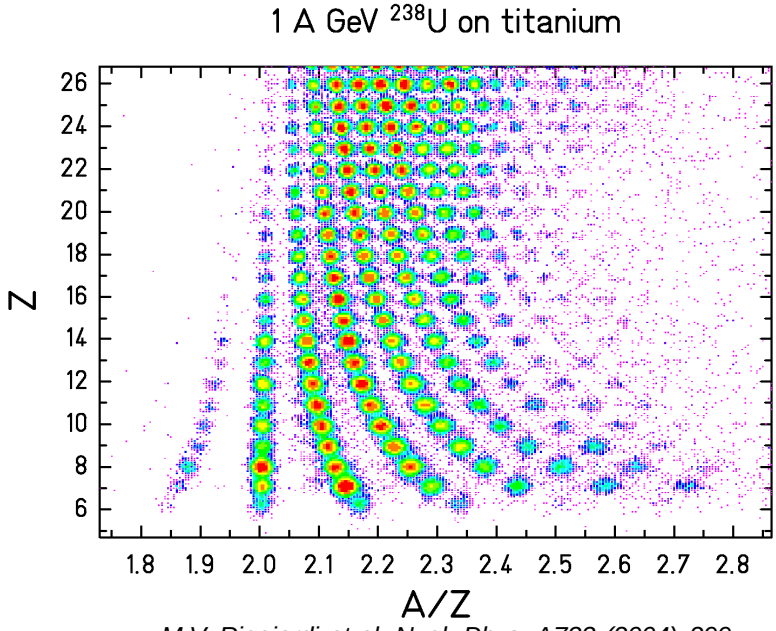

M.V. Ricciardi et al.,Nucl. Phys. A733 (2004) 299.

Optimum energy for FRS-like momentum achromat

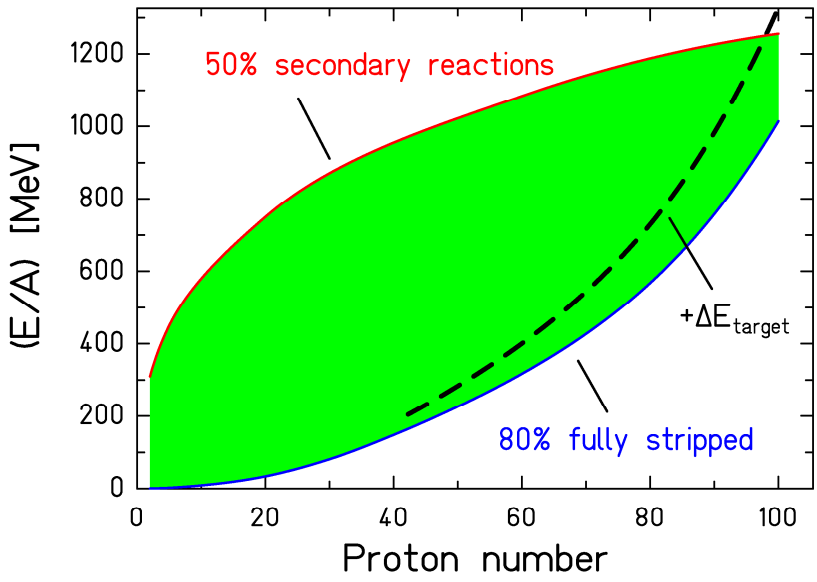

K.H. Schmidt, Euroschool Leuven 2000.

BigRIPS at RIKEN, Japan

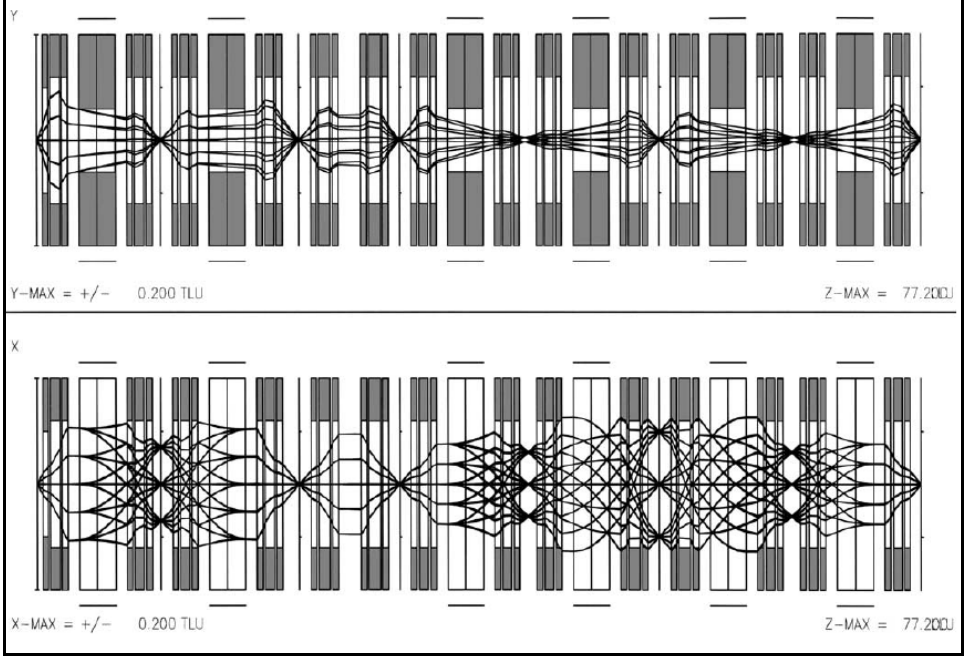

BigRIPS at RIKEN, Japan

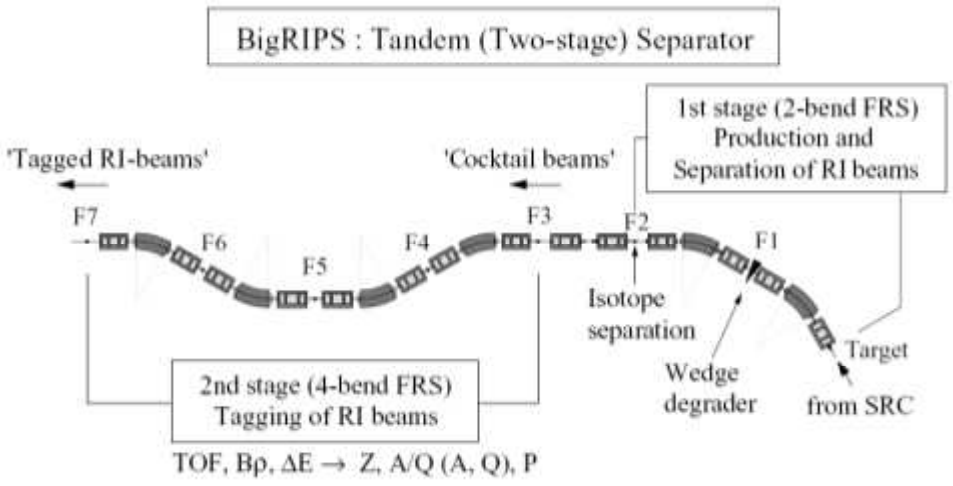

T. Kubo, Nucl. Instr. Meth. B204 (2003) 97.

Super-FRS at FAIR, Darmstadt

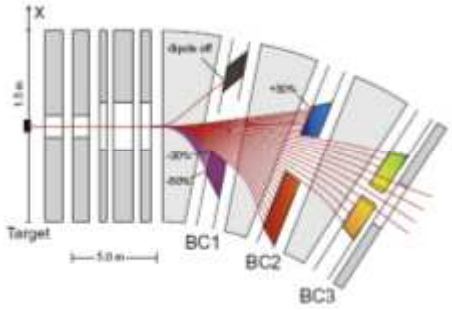

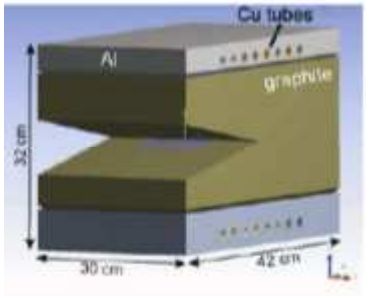

Fig. 4. Beam catcher locations in the first dipole stage of the pre-separator. Depending on the fragment setting the primary beam will be dumped at the position given by the relative difference in magnetic rigidity. Plotted are trajectories of primary beams with different $\delta_{B\rho}$ values in steps of 1%.

Fig. 5. Layout of the front part of the beam catcher. The V-shaped graphite block will absorb the beam energy of up to 50 kW and is actively cooled.

M. Winkler et al., Nucl. Instr. Meth. B266 (2008) 4183.

Q3D Spectrometer

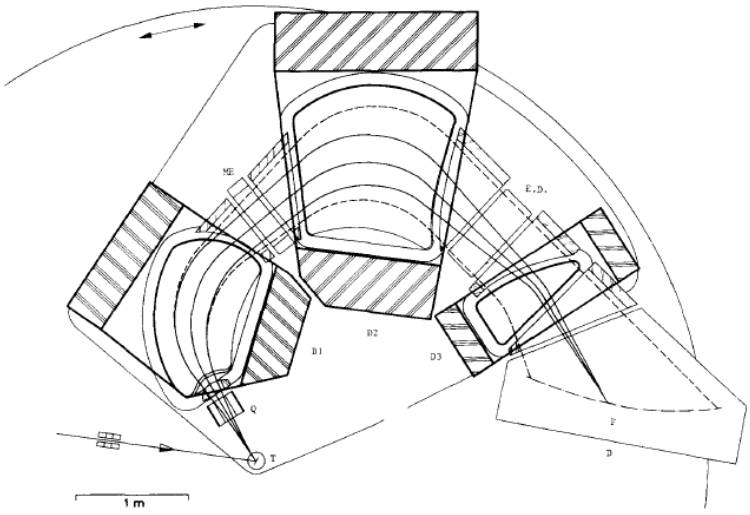

Fig. 1. Ion optical layout of the QDDD spectrograph. T – target chamber; ME – multipole element; D1, D2, D3 – dipole magnets; E.D. – electrostatic deflector; F – focal surface; D – detector chamber.

M. Löffler et al., Nucl. Instr. Meth. 111 (1973) 1.

Example spectrum ^{180}Hf(d,p)

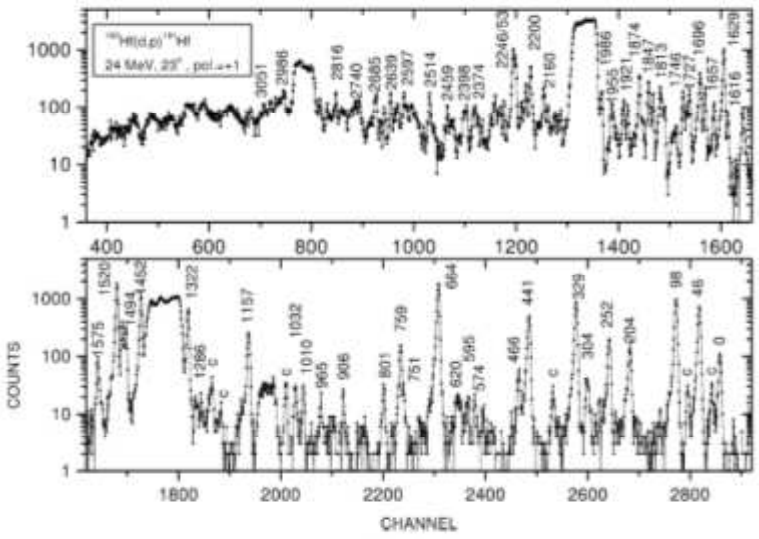

Fig. 3. An example of proton spectra from the reaction ^{180}Hf(d, p)^{181}Hf. The peaks are labelled by the excitation energy in keV. The proton groups labeled with 'c' belong to contaminant isotopes.

The SPEG spectrometer at GANIL

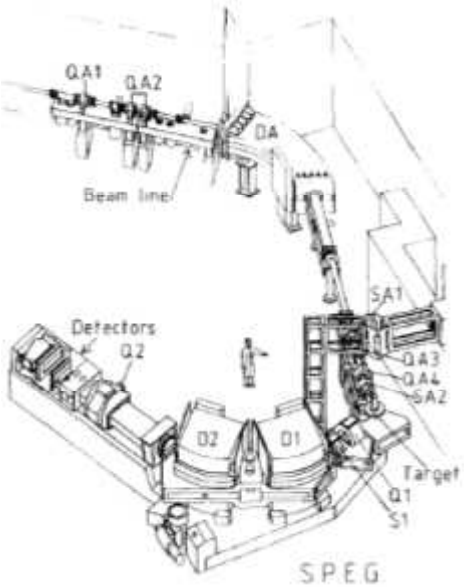

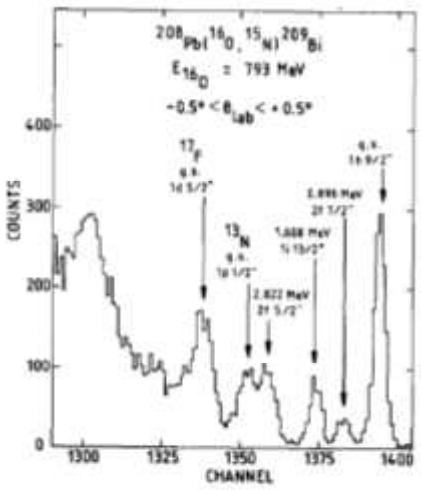

Fig. 20. Zero degree spectrum measured for the ^{208}Pb(^{16}O, ^{15}N)^{209}Bi reaction.

L. Bianchi et al., Nucl. Instr. Meth. A276 (1989) 509.

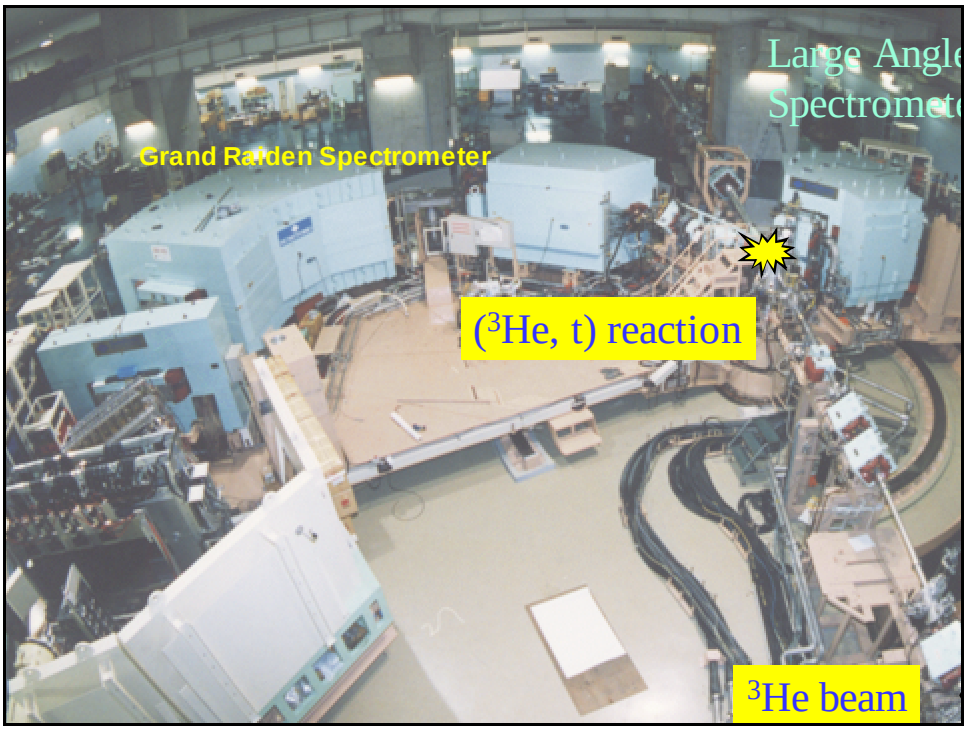

Beam line WS-course at RCNP

T. Wakasa et al., NIM A482 ('02) 79.

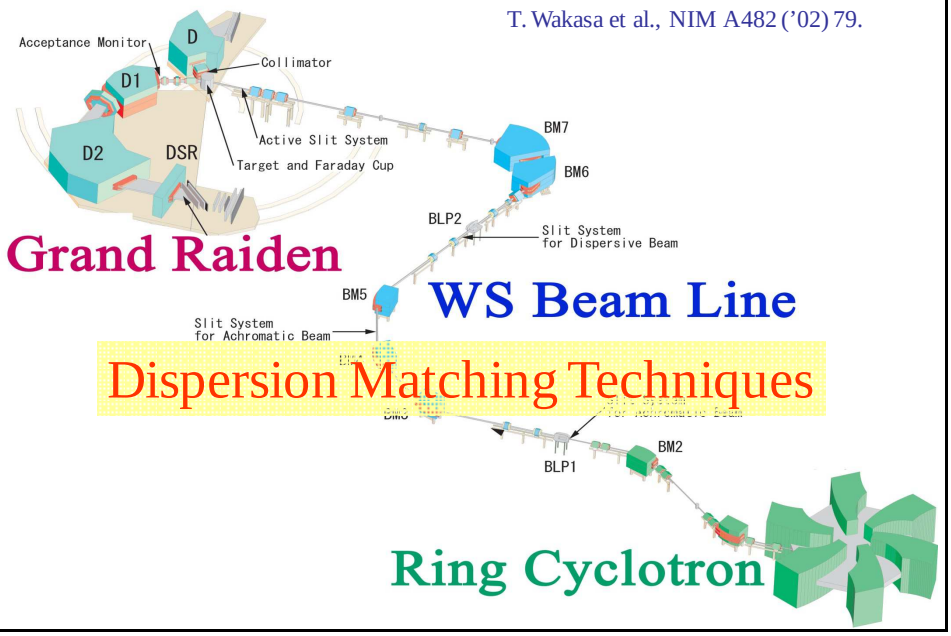

^{9}Be(^{3}He,t)^{9}B spectrum (at various scales)

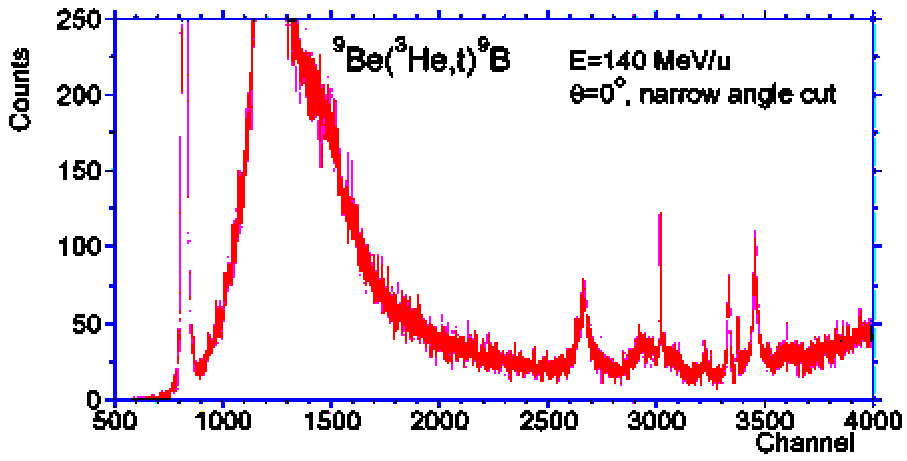

Y. Fujita

^{9}Be(^{3}He,t)^{9}B spectrum (II)

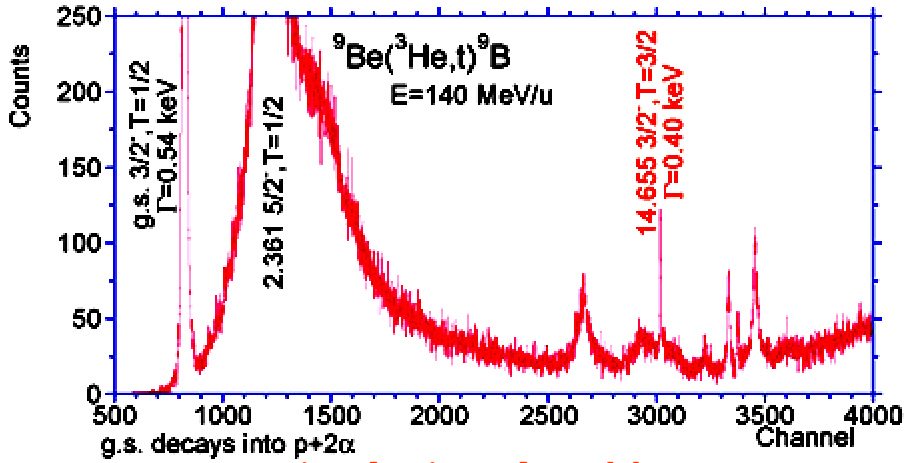

Isospin selection rule prohibits **proton decay** of **T=3/2** state!

C. Scholl, Köln

Outline

1. **Definitions and history**
2. **Basics of ion optics and dispersive elements**
3. **Static fields**
   a) deflection spectrometer
   b) retardation spectrometer
4. **Dynamic fields/separation**
   a) Time-of-Flight spectrometer
   b) Radiofrequency spectrometer
   c) Traps
5. **Technical realization (ion sources, etc.)**
6. **"Real examples" for nuclear physics applications**
   a) ISOL
   b) Recoil separators
   c) Fragment separators
   d) Spectrometer

References

- **Inorganic Mass Spectrometry: Principles and Applications, Sabine Becker, Wiley, 2007.**
- **Optics of Charged Particles, Hermann Wollnik, Academic Press 1987.**
- **Mass spectroscopy, H.E. Duckworth et al., Cambridge Univ. Press, 1986.**
- **The transport of charged particle beams, A.P. Banford, E. & F.N. Spon, 1966.**
- **Proceedings of the EMIS (Electromagnetic Isotope Separation) Conferences:**
  Nucl. Instr. Meth. B266, NIM B204, NIM B126, NIM B70, …